Journal of the Mechanics and Physics of Solids 144 (2020) 104107

Contents lists available at ScienceDirect

Journal of the Mechanics and Physics of Solids

journal homepage: www.elsevier.com/locate/jmps

Microtwist elasticity: A continuum approach to zero modes and topological polarization in Kagome lattices

Hussein Nassar*, Hui Chen*, Guoliang Huang*

Department of Mechanical and Aerospace Engineering, University of Missouri, Columbia, Missouri 65211, USA

ARTICLE INFO

Article history:
Received 2 April 2020
Revised 22 July 2020
Accepted 30 July 2020
Available online 5 August 2020

Keywords:
Zero modes
Topological polarization
Kagome lattices
Isostatic lattices
Microtwist continuum
Effective medium theory
Mechanics of generalized continua

ABSTRACT

The topologically polarized isostatic lattices discovered by Kane and Lubensky (2014, Nat. Phys. 10, 39–45) challenged the standard effective medium theories used in the modeling of many truss-based materials and metamaterials. As a matter of fact, these exhibit Parity (P) asymmetric distributions of zero modes that induce a P-asymmetric elastic behavior, both of which cannot be reproduced within Cauchy elasticity. Here, we propose a new effective medium theory baptized "microtwist elasticity" capable of rendering polarization effects on a macroscopic scale. The theory is valid for trusses on the brink of a polarized-unpolarized phase transition in which case they necessarily exhibit more periodic zero modes than they have dimensions. By mapping each periodic zero mode to a macroscopic degree of freedom, the microtwist theory ends up being a kinematically enriched theory. Microtwist elasticity is constructed thanks to leading order two-scale asymptotics and its constitutive and balance equations are derived for a fairly generic isostatic truss: the Kagome lattice. Various numerical and analytical calculations, of the shape and distribution of zero modes, of dispersion diagrams and of polarization effects, systematically show the quality of the proposed effective medium theory.

1. Introduction

Periodic trusses are potent idealized models of several materials such as foams, crystals and metamaterials. When the truss has poor connectivity, the material exhibits a number of zero modes, i.e., deformation modes that cost little to no elastic energy. While catastrophic in many cases, zero modes can still be desirable. In auxetics, for instance, reentrant structures with approximate zero modes provided some of the first examples of materials with negative Poisson's ratio (Lakes, 1987). In applications related to smart materials and robotics, non-linear zero modes are essential in structures that can deploy, morph, adapt and move (Milton, 2013a, 2013b, Nassar et al., 2017, 2018; Peraza-Hernandez et al., 2014; Rocklin et al., 2017; Rus and Tolley, 2018). But perhaps the most spectacular application of zero modes in recent years has been in the design of acoustic "invisibility" cloaks. Indeed, form-invariance, a cornerstone of transformation-based cloaking, can only be fulfilled thanks to materials with a number of non-trivial zero modes. In acoustics, Norris (2008) identified these materials to be Milton and Cherkaev's (1995) pentamodes; in full elasticity, other materials with zero modes are just as useful (Nassar et al., 2018a; 2019; 2020; Xu et al., 2020).

* Corresponding authors.
E-mail addresses: nassarh@missouri.edu (H. Nassar), hc6xc@mail.missouri.edu (H. Chen), huangg@missouri.edu (G. Huang).

https://doi.org/10.1016/j.jmps.2020.104107
0022-5096/

Nomenclature

$\langle \cdot, \cdot \rangle$	The dot product
$\boldsymbol{\nabla}$, $\boldsymbol{\nabla}^s$	Gradient and symmetrized gradient operators
$\bar{\cdot}$	Rotation through $\pi/2$
$\cdot'$	Conjugate transpose, adjoint
δ, δ^2	Prefixes for first and second order corrections
$\boldsymbol{\sigma}$, $\boldsymbol{\varepsilon}$	Stress and strain tensors
$\mathbf{C}^*$, $\mathbf{C}$	Effective Cauchy and microtwist elasticity tensors
ϵ^*, ϵ	Effective Cauchy and microtwist strain energy densities
$j = 1, 2, 3$	Index of lattice vectors, nodes and bonds
(l, m, n)	Unit cell index
$\mathbf{r}_j$, $\mathbf{e}_j$	Dimensional and normalized lattice vectors
$\mathbf{e}_{j\ldots j}$	Tensorial powers of $\mathbf{e}_j$
$\mathbf{x}_j^{l,m,n}$, $\mathbf{x}_j$	Position of node j
$\mathbf{u}_j^{l,m,n}$, $\mathbf{u}_j$	Displacement of node j
$\mathbf{m}_j$, $\mathbf{n}_j$	Unit vectors orienting the bonds
a_j, b_j	Bond lengths
$y_j^{l,m,n}$, $z_j^{l,m,n}$	Bond elongations
α_j, β_j	Bond spring constants
$\mathbf{t}_j^{l,m,n}$, $\mathbf{f}_j^{l,m,n}$	Internal and external nodal forces
m_j	Mass of node j
γ	Similarity ratio
Δ	Triangle whose vertices are nodes 1, 2 and 3
h_j	Height of node j in triangle Δ
$\mathbf{d}$	Position vector of the center of mass of triangle Δ
$\mathbf{q}$, ω	Wavenumber and angular frequency
q_j, Q_j, ∂_j	Wavenumber component, unitary complex phase factor and partial derivative in direction $\mathbf{r}_j$
C_0, $C(\mathbf{q})$	Compatibility matrices
Φ	Column vector of nodal displacements
$\mathbf{I}$	Second-order identity tensor
D, T	Mode shapes of translation and periodic twisting
w_j	Distortion parameters
K, M, C	Rigidity, mass and compatibility operators
F	External forces column vector
$\mathbf{F}$, τ	Resultant body force and torque
ρ, η	Effective mass and moment of inertia densities
$\mathbf{B}$, $\mathbf{M}$, $\mathbf{D}$, $\mathbf{A}$, L	Effective constitutive tensors
k_j	Equivalent spring constant
$\boldsymbol{\xi}$, s	Couple stress and hyperstress
Ω, $\partial\Omega$, $\mathbf{N}$	A domain, its boundary and the outward unit normal
κ	Effective torsional spring constant of elastic hinges
$\mathbf{e}_x$, $\mathbf{e}_y$	Cartesian basis vectors
$\mathbf{x}$, x, y	Continuous space variables
$\mathbf{U}$, φ	Macroscopic fields of displacement and twisting
$\mathbf{U}_o$, φ_o	Translation and twisting amplitudes
U_x, U_y	Displacement components
$U_{x,x}$, $\varphi_{,y}$, ...	Partial derivatives
q_x, q_y	Cartesian coordinates of wavenumber $\mathbf{q}$
q_R, q_I	Real and imaginary parts of component q_y
r	Decay factor of localized zero mode
Z	Number of zero modes
ζ	Inclination of $\mathbf{e}_y$ with respect to $\mathbf{e}_1$
$\mathbf{P}$, $\mathbf{P}^{KL}$	Topological polarization vectors

From the point of view of the material's constitutive law $\boldsymbol{\sigma} = \mathbf{C}^* : \boldsymbol{\varepsilon}$, zero modes appear when the effective elasticity tensor $\mathbf{C}^*$ is singular. Thus, zero modes correspond to compatible fields of strain $\boldsymbol{\varepsilon}_o(\mathbf{x})$ such that $\mathbf{C}^* : \boldsymbol{\varepsilon}_o = \mathbf{0}$ at each position $\mathbf{x}$. Remarkably, if $\boldsymbol{\varepsilon}_o(\mathbf{x})$ is a zero mode then so is $\boldsymbol{\varepsilon}_o(-\mathbf{x})$. More generally, Parity (P) symmetry, namely the invariance

of the set of solutions under the spatial inversion $\mathbf{x} \mapsto -\mathbf{x}$, is a key feature of Cauchy's theory of elasticity. Nonetheless, there are trusses where zero modes systematically grow in amplitude in a preferential direction and systematically decay in the opposite direction (Lubensky et al., 2015; Mao and Lubensky, 2018). Materials with such underlying trusses have a broken P-symmetry; we say that they are polarized. Other trusses admit zero modes for which $\boldsymbol{\varepsilon}_0(\mathbf{x}) = \mathbf{0}$ (see, e.g., the same references). To capture such zero modes on the level of the material requires finer measures of strain besides $\boldsymbol{\varepsilon}$ and its gradients. In both cases, Cauchy's theory is unsatisfactory. It is the purpose of the present paper to propose an enriched effective medium theory capable of faithfully reproducing microstructural zero modes and related polarization effects on the continuum scale. Derivations are carried for a fairly generic truss: the Kagome lattice.

Polarized Kagome lattices came to our attention while reading the elegant work of Kane and Lubensky (2014) on topological polarization in isostatic lattices. In the detail, a regular, e.g. the standard, Kagome lattice exhibits bulk zero modes which maintain uniform amplitude across the whole truss. These take the form of zero-frequency Floquet-Bloch eigenmodes of a given wavenumber. General geometric distortions of the lattice then opens a partial bandgap about the zero frequency and block these modes at non-zero wavenumbers. Hence, zero modes become "evanescent"; they adopt exponential profiles that decay towards the bulk and re-localize at free boundaries. Kane and Lubensky characterized the conditions under which the re-localization of zero modes towards the free boundaries of a distorted lattice happens unevenly and favors certain boundaries over their opposites. Note that the found conditions and the resulting P-asymmetric distribution of zero modes are topological in nature, i.e., they are immune to continuous perturbations, small and large, so long as the aforementioned zero-frequency gap remains open. This is why such Kagome lattices are qualified as "topologically polarized". Based on these principles, Bilal et al. (2017) designed and tested a material featuring a polarized elastic behavior. A finite slab of their material appears soft when indented on one side and hard when indented on the opposite side. Elastic polarization effects are not restricted to boundaries and emerge in the bulk as well; see, e.g., Rocklin (2017).

Our aim therefore is to reconcile the above observations with an effective theory of elasticity. Following asymptotic analysis, we find that the theory naturally maps the periodic zero modes of the truss to macroscopic Degrees Of Freedom (DOFs). For instance, regular Kagome lattices admit three periodic zero modes, two translations and the so-called periodic twisting. While translations are mapped to the macroscopic displacement field $\mathbf{U}$, periodic twisting is mapped to an extra DOF φ. The resulting effective continuum is called the "microtwist" continuum after the additional periodic zero mode. The microtwist continuum also has two extra measures of strain, φ itself and its gradient, and by way of duality, two extra measures of stress. By continuity, nearly-regular or weakly-distorted Kagome lattices are also described in the same way albeit with different effective properties. In that case, periodic twisting is no longer a zero mode strictly speaking but still corresponds to a highly compliant mechanism. By contrast, we do not deal with strongly-distorted lattices: these may exhibit strong polarization effects but only within thin boundary layers. We speculate that Cauchy elasticity with ad-hoc boundary or jump conditions is satisfactory for their continuum modeling; see, e.g., the papers by Marigo and Maurel (2016, 2017).

Microtwist elasticity is the outcome of leading order two-scale asymptotic expansions. It is reminiscent of "$\mathbf{k} \cdot \mathbf{p}$" perturbation theory used in condensed matter physics (Dresselhaus et al., 2008). In that language, the theory describes the asymptotic behavior of Kagome lattices near the Γ point when the acoustic branches and the first optical branch are strongly coupled, i.e., degenerate or nearly degenerate. Furthermore, the theory bears resemblance to high-frequency asymptotic homogenization theories (see, e.g., Allaire et al., 2011; Bensoussan et al., 1978; Craster et al., 2010; Harutyunyan et al., 2016; Makwana et al., 2016).

Several earlier contributions sought generalized effective media for trusses, be them of the micropolar type (Bacigalupo and Gambarotta, 2014; Chen et al., 2014; Frenzel et al., 2017; Lakes, 2001; Lakes and Benedict, 1982; Liu et al., 2012; Spadoni and Ruzzene, 2012) or the strain gradient type (Auffray et al., 2010; Bacigalupo and Gambarotta, 2014; Rosi and Auffray, 2016). Often, the aim was to model chiral effects. In that regard, it is worth stressing that chirality, or anisotropy of any kind for that matter, is fundamentally different from P-asymmetry. Indeed, when the former is concerned with the action of rotations on the constitutive law, the latter is concerned with the action of the inversion $\mathbf{x} \mapsto -\mathbf{x}$ on fields solution to the motion equation. See, e.g., Nassar et al. (2020) for a theory of elasticity that is chiral but P-symmetric. More relevant to our purposes is the work of Sun et al. (2012) who hinted at microtwist elasticity in a particular case but did not pursue a full theory. More recently, Sun and Mao (2019) and Saremi and Rocklin (2020) proposed theories for polarized effective media of the strain gradient type. Our asymptotic analysis suggests that a kinematically enriched medium is indispensable, at least in the strong coupling limit of interest here.

The paper goes as follows: in Section 2, we classify general Kagome lattices in two phases, regular and distorted, based on a count of their periodic and Floquet-Bloch zero modes. In Section 3, we argue why enriching the effective medium is necessary in the case of regular and weakly-distorted lattices. Subsequently, we deploy two-scale asymptotics and deduce, in closed form, the constitutive and balance equations governing the effective microtwist continuum. In Section 4, we compare and assess both microtwist and Cauchy's elasticity in reference to the dispersion diagrams of a class of equilateral Kagome lattices. Section 5 is dedicated to the study of polarization effects, be them topological or not. Most importantly, we demonstrate how the microtwist theory predicts the onset of polarization in the elastic behavior of Kagome lattices thanks to its generalized effective elasticity tensors and provides an accurate continuum version of the topological polarization vector of Kane and Lubensky (2014). In contrast to discrete methods, we hope that the present theory will provide corrections to the continuum models of strength of materials widely used by engineers in cases where the constitutive materials are lattice-like; the theory should also enrich the space of accessible constitutive behaviors so as to permit solving wider classes of materials inverse design problems.

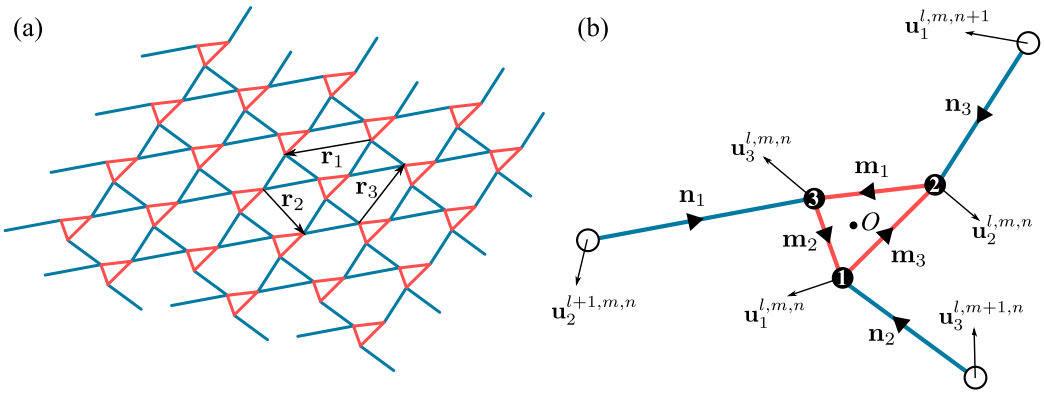

Fig. 1. A general Kagome lattice: (a) a periodic reference configuration; (b) a magnified and annotated unit cell. The displacements of the nodes are shown as arrows. The solid and empty circles represent the interior and exterior nodes of the unit cell respectively. Blue bonds with unit vectors $\mathbf{m}_j$ and red bonds with unit vectors $\mathbf{n}_j$ have respective lengths a_j and b_j and respective spring constants α_j and β_j. (For interpretation of the references to colour in this figure legend, the reader is referred to the web version of this article.)

2. Kagome lattices and their zero modes

General Kagome lattices are introduced and classified into two phases, regular and distorted, based on the number and type of zero modes they support. The analysis here is based on the discrete lattice model. A continuum model, suitable for regular and weakly-distorted lattices, will be derived in the next section.

2.1. Kinematics and dynamics of Kagome lattices

Consider the general Kagome lattice depicted in Fig. 1a in a periodic reference configuration. The lattice is made of a set of massless spring-like edges connecting massive hinge-like nodes. Vectors $\mathbf{r}_j$ are lattice vectors: the reference configuration is invariant by translation along any integer linear combination of the $\mathbf{r}_j$. A unit cell is shown on Fig. 1b: it has three nodes in its interior, i.e., the filled circles, indexed with $j \in \{1, 2, 3\}$ and initially placed at $\mathbf{x}_j$. Index j is always understood modulo 3: if $j = 3$ then $j + 1 = 1$ and if $j = 1$ then $j - 1 = 3$. Exterior to the unit cell, but at its boundary, there are three other nodes drawn as empty circles and whose initial positions are given by $\mathbf{x}_j + \mathbf{r}_{j-1}$. Thus, the initial positions of all nodes can be deduced from the $\mathbf{x}_j$ according to

$$\mathbf{x}_j^{l,m,n} = \mathbf{x}_j + \mathbf{x}^{l,m,n}, \quad \mathbf{x}^{l,m,n} = l\mathbf{r}_1 + m\mathbf{r}_2 + n\mathbf{r}_3, \quad (l, m, n) \in \mathbb{Z}^3. \tag{1}$$

Here, $\mathbf{x}_j^{l,m,n}$ designates the position of node j of unit cell (l, m, n). The use of three indices, l, m and n, to describe a 2D lattice may seem superfluous. Indeed, one has $\mathbf{r}_1 + \mathbf{r}_2 + \mathbf{r}_3 = \mathbf{0}$ and any combination of $\mathbf{r}_1$, $\mathbf{r}_2$ and $\mathbf{r}_3$ can be reduced to one where, say, only $\mathbf{r}_1$ and $\mathbf{r}_2$ are present. Nonetheless, in order to enforce the formal permutation symmetry, namely that the nodes within a unit cell play equivalent roles and can be numbered arbitrarily, it is preferable to maintain the use of three vectors $\mathbf{r}_j$ without expanding any one along the other two. This attitude will greatly simplify later derivations. Note that, as a side effect, the coordinates (l, m, n) of a unit cell are not unique. For instance, (0,0,0) and (1,1,1) designate the same unit cell. If uniqueness is desired, then one can require the satisfaction of some constraint[1] such as $0 \le l + m + n \le 2$ but this will not be enforced and should have no influence on what follows.

The displacement of node j in unit cell (l, m, n) is called $\mathbf{u}_j^{l,m,n}$. A unit cell has three nodes and therefore a total of six DOFs. A unit cell further has six edges oriented along the unit vectors $\mathbf{m}_j$ (red bonds) and $\mathbf{n}_j$ (blue bonds) and of respective lengths a_j and b_j; see Fig. 1b. The Kagome lattice is therefore isostatic in the sense that it has as much DOFs as it has bonds per unit cell. The elongation of the edge along $\mathbf{m}_j$ (resp. $\mathbf{n}_j$) is called $y_j^{l,m,n}$ (resp. $z_j^{l,m,n}$). Displacements yield elongations according to the relations

$$\begin{aligned} y_j^{l,m,n} &= \left\langle \mathbf{m}_j, \mathbf{u}_{j-1}^{l,m,n} - \mathbf{u}_{j+1}^{l,m,n} \right\rangle, & z_1^{l,m,n} &= \left\langle \mathbf{n}_1, \mathbf{u}_3^{l,m,n} - \mathbf{u}_2^{l+1,m,n} \right\rangle, \\ z_2^{l,m,n} &= \left\langle \mathbf{n}_2, \mathbf{u}_1^{l,m,n} - \mathbf{u}_3^{l,m+1,n} \right\rangle, & z_3^{l,m,n} &= \left\langle \mathbf{n}_3, \mathbf{u}_2^{l,m,n} - \mathbf{u}_1^{l,m,n+1} \right\rangle. \end{aligned} \tag{2}$$

[1] Let (L, M, N) designate a unit cell, then any triplet $(l, m, n) \equiv (L + d, M + d, N + d)$ designates the same cell. Now the integer interval $[-L - M - N, 2 - L - M - N]$ is of length 3 and thus necessarily contains a multiple of 3; let that multiple be $3d$. The resulting triplet (l, m, n) satisfies the prescribed constraint; furthermore, since d is unique, so is (l, m, n).

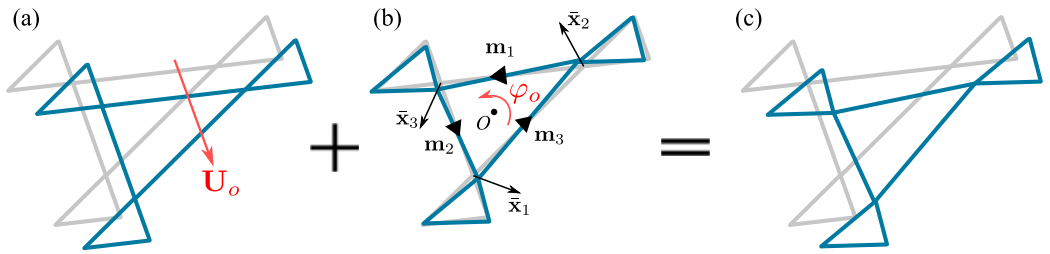

Fig. 2. Generic periodic zero mode of a regular Kagome lattice: (a) global translation $\mathbf{U}_o$; (b) a twisting motion of angle φ_o around the center O; (c) a linear combination of a translation and a twisting motion. The initial and deformed configurations are traced in grey and blue respectively. (For interpretation of the references to colour in this figure legend, the reader is referred to the web version of this article.)

The tensions in the corresponding edges are given by $\alpha_j y_j^{l,m,n}$ and $\beta_j z_j^{l,m,n}$ where α_j and β_j are the spring constants of edges $\mathbf{m}_j$ and $\mathbf{n}_j$ respectively. Thus, the internal force $\mathbf{t}_j^{l,m,n}$ acting on node j in unit cell (l, m, n) reads

$$\begin{aligned}
\mathbf{t}_1^{l,m,n} &= -\alpha_2 y_2^{l,m,n}\mathbf{m}_2 - \beta_2 z_2^{l,m,n}\mathbf{n}_2 + \alpha_3 y_3^{l,m,n}\mathbf{m}_3 + \beta_3 z_3^{l,m,n-1}\mathbf{n}_3,\\
\mathbf{t}_2^{l,m,n} &= -\alpha_3 y_3^{l,m,n}\mathbf{m}_3 - \beta_3 z_3^{l,m,n}\mathbf{n}_3 + \alpha_1 y_1^{l,m,n}\mathbf{m}_1 + \beta_1 z_1^{l-1,m,n}\mathbf{n}_1,\\
\mathbf{t}_3^{l,m,n} &= -\alpha_1 y_1^{l,m,n}\mathbf{m}_1 - \beta_1 z_1^{l,m,n}\mathbf{n}_1 + \alpha_2 y_2^{l,m,n}\mathbf{m}_2 + \beta_2 z_2^{l,m-1,n}\mathbf{n}_2.
\end{aligned} \tag{3}$$

Finally, Newton's second law can be stated as

$$\mathbf{t}_j^{l,m,n} + \mathbf{f}_j^{l,m,n} = m_j \ddot{\mathbf{u}}_j^{l,m,n}, \tag{4}$$

where m_j is the mass of node j and $\mathbf{f}_j^{l,m,n}$ is an external force applied to node j of unit cell (l, m, n).

In what follows, without loss of generality, we let the origin of coordinates "O" be the geometric center of the red triangle $\Delta \equiv (a_1\mathbf{m}_1, a_2\mathbf{m}_2, a_3\mathbf{m}_3)$. Accordingly, the reference positions of the three interior nodes, with respect to the origin, are

$$\mathbf{x}_j = \frac{a_{j+1}\mathbf{m}_{j+1} - a_{j-1}\mathbf{m}_{j-1}}{3}. \tag{5}$$

For later purposes, we also define $\bar{\mathbf{x}}_j$ to be the image of $\mathbf{x}_j$ by a plane rotation of angle $\pi/2$. More generally, a superimposed bar will symbolize a plane rotation of $\pi/2$.

2.2. Zero modes

We call *zero mode*, a static displacement solution to Newton's equation in the absence of external loading, i.e., a solution $\mathbf{u}_j^{l,m,n}$ to

$$\mathbf{t}_j^{l,m,n} = \mathbf{0}. \tag{6}$$

Equivalently, a zero mode is a configuration of the lattice which stretches and compresses no bonds so that

$$y_j^{l,m,n} = z_j^{l,m,n} = 0. \tag{7}$$

In this sense, rigid body translations and rotations are zero modes. Kagome lattices admit a number of other, more interesting, zero modes all inherited from the elementary *twisting* mechanism illustrated on Fig. 2. Understanding the zero modes of Kagome lattices is essential to justify the need for the generalized theory of elasticity introduced in the next section. Thus, zero modes are studied in the remainder of this section in some detail. This is also an occasion to gain insight into the geometry of Kagome lattices and to familiarize the reader with the introduced notations. In particular, we will investigate periodic and Floquet-Bloch zero modes.

2.3. Periodic zero modes

We call *periodic*[2] a configuration that does not depend on the indices (l, m, n) of unit cells, i.e.,

$$\mathbf{u}_j^{l,m,n} = \mathbf{u}_j. \tag{8}$$

[2] Periodicity here is reserved for invariance by translation along the lattice vectors $\mathbf{r}_j$. Mode shapes that are invariant by translation along some other vectors will not be referred to as periodic. Equivalently, only modes with a vanishing wavenumber (modulo the reciprocal lattice) are qualified as periodic.

Zero mode or not, dismissing the dependence over (l, m, n) greatly simplifies the governing equations. For instance, elongations are given by the matrix product

$$\begin{bmatrix} y_1 \\ y_2 \\ y_3 \\ z_1 \\ z_2 \\ z_3 \end{bmatrix} = C_0 \begin{bmatrix} \mathbf{u}_1 \\ \mathbf{u}_2 \\ \mathbf{u}_3 \end{bmatrix}, \quad C_0 = \begin{bmatrix} \mathbf{0} & -\mathbf{m}_1' & \mathbf{m}_1' \\ \mathbf{m}_2' & \mathbf{0} & -\mathbf{m}_2' \\ -\mathbf{m}_3' & \mathbf{m}_3' & \mathbf{0} \\ \mathbf{0} & -\mathbf{n}_1' & \mathbf{n}_1' \\ \mathbf{n}_2' & \mathbf{0} & -\mathbf{n}_2' \\ -\mathbf{n}_3' & \mathbf{n}_3' & \mathbf{0} \end{bmatrix}, \tag{9}$$

where C_0 is a 6×6 compatibility matrix and a prime means conjugate transpose so that $\mathbf{m}_j' \mathbf{u}_k = \langle \mathbf{m}_j, \mathbf{u}_k \rangle$. Accordingly, a periodic zero mode solves

$$C_0 \Phi = 0, \quad \Phi = \begin{bmatrix} \mathbf{u}_1 \\ \mathbf{u}_2 \\ \mathbf{u}_3 \end{bmatrix}. \tag{10}$$

Hence, periodic zero modes are null vectors of matrix C_0. By the rank-nullity theorem (Birkhoff and MacLane, 1998), their number is equal to $Z = 6 - \text{rank}C_0$ where 6 is the dimension of C_0 and $\text{rank}C_0$ is its rank.

Translations by a vector $\mathbf{U}_o$ are characterized by $\mathbf{u}_1 = \mathbf{u}_2 = \mathbf{u}_3 = \mathbf{U}_o$ (Fig. 2a). They take the form

$$\Phi = \begin{bmatrix} \mathbf{U}_o \\ \mathbf{U}_o \\ \mathbf{U}_o \end{bmatrix} = D\mathbf{U}_o, \quad D = \begin{bmatrix} \mathbf{I} \\ \mathbf{I} \\ \mathbf{I} \end{bmatrix}, \tag{11}$$

where $\mathbf{I}$ is the second-order identity tensor. These clearly satisfy $C_0 \Phi = 0$. Translations span two periodic zero modes. It is not too hard to show that if $\mathbf{m}_j \neq -\mathbf{n}_j$, for some j, then $\text{rank}C_0 = 4$ and $Z = 2$. Such lattices will be called *distorted*: they admit no other periodic zero modes besides translations (Appendix A). Otherwise, if $\mathbf{m}_j = -\mathbf{n}_j$, for all j, then $\text{rank}C_0 = 3$ and $Z = 3$. Such lattices will be called *regular*. These admit one extra periodic zero mode given by the twisting motion

$$\Phi = \begin{bmatrix} \bar{\mathbf{x}}_1 \\ \bar{\mathbf{x}}_2 \\ \bar{\mathbf{x}}_3 \end{bmatrix} \varphi_o \equiv T\varphi_o. \tag{12}$$

Restricted to the nodes of one unit cell, twisting is a rotation whose center can be chosen arbitrarily. Here, the geometric center "O" is chosen as the center of rotation whereas φ_o is the angle of rotation (Fig. 2b). It is easy to check that T is indeed a zero mode, i.e., that $C_0 T = 0$. While doing so it is useful to verify first that $\bar{\mathbf{x}}_{j-1} - \bar{\mathbf{x}}_{j+1} = a_j \bar{\mathbf{m}}_j$ is orthogonal to both $\mathbf{m}_j$ and $\mathbf{n}_j$, these two being parallel in regular lattices.

In conclusion, the periodic zero modes of a regular Kagome lattice are given by the linear combination of translations and a twisting motion (Fig. 2c)

$$\Phi = D\mathbf{U}_o + T\varphi_o, \tag{13}$$

or equivalently by

$$\mathbf{u}_j = \mathbf{U}_o + \varphi_o \bar{\mathbf{x}}_j. \tag{14}$$

2.4. Floquet-Bloch zero modes

Floquet-Bloch zero modes take the form

$$\mathbf{u}_j^{l,m,n} = \mathbf{u}_j \exp\left(i\langle \mathbf{q}, \mathbf{x}^{l,m,n} \rangle\right) \tag{15}$$

where $\mathbf{q}$ is a real wavenumber. Alternatively, with $\mathbf{x}^{l,m,n} = l\mathbf{r}_1 + m\mathbf{r}_2 + n\mathbf{r}_3$, we can write

$$\mathbf{u}_j^{l,m,n} = Q_1^l Q_2^m Q_3^n \mathbf{u}_j, \tag{16}$$

with $Q_j \equiv e^{iq_j}$ and $q_j \equiv \langle \mathbf{q}, \mathbf{r}_j \rangle$. In particular, the Q_j are unitary complex numbers such that

$$Q_1 Q_2 Q_3 = \exp\left(i\langle \mathbf{q}, \mathbf{r}_1 + \mathbf{r}_2 + \mathbf{r}_3 \rangle\right) = 1. \tag{17}$$

Elongations admit similar expressions

$$y_j^{l,m,n} = Q_1^l Q_2^m Q_3^n y_j, \quad z_j^{l,m,n} = Q_1^l Q_2^m Q_3^n z_j, \tag{18}$$

and it is again convenient to introduce a compatibility matrix as in (9) but with C_0 replaced by

$$C(\mathbf{q}) = \begin{bmatrix} \mathbf{0} & -\mathbf{m}_1' & \mathbf{m}_1' \\ \mathbf{m}_2' & \mathbf{0} & -\mathbf{m}_2' \\ -\mathbf{m}_3' & \mathbf{m}_3' & \mathbf{0} \\ \mathbf{0} & -Q_1\mathbf{n}_1' & \mathbf{n}_1' \\ \mathbf{n}_2' & \mathbf{0} & -Q_2\mathbf{n}_2' \\ -Q_3\mathbf{n}_3' & \mathbf{n}_3' & \mathbf{0} \end{bmatrix}. \tag{19}$$

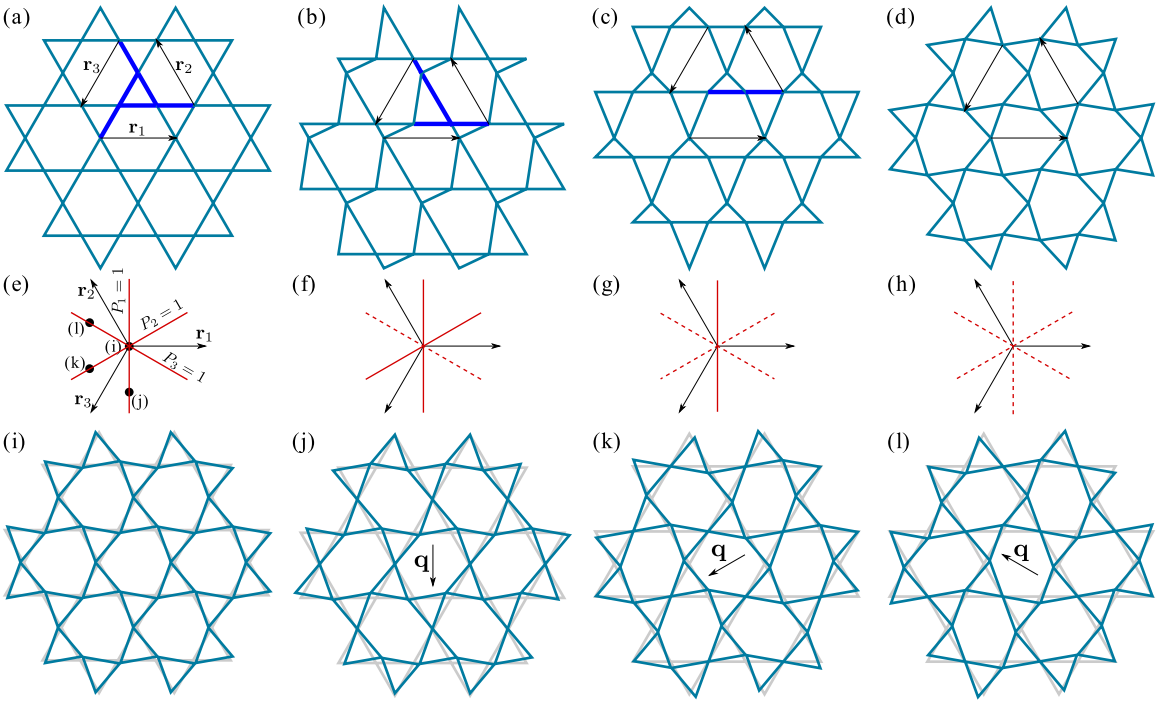

Fig. 3. Examples of regular (a) and distorted Kagome lattices (b-d). Blue solid lines correspond to pairs of colinear bonds (i.e., $\mathbf{m}_j = -\mathbf{n}_j$) in the unit cell. Their zero frequency contours are depicted on (e-h); red solid lines correspond to actual zero modes; red dashed lines correspond to modes that have disappeared due to the alignment-breaking distortion. Examples of Floquet-Bloch zero modes acting on the regular lattice (a) are shown in (i-l): (i) periodic zero mode ($\mathbf{q} = \mathbf{0}$); (j-l) Floquet-Bloch zero modes with $\mathbf{q} \perp \mathbf{r}_j$. (For interpretation of the references to colour in this figure legend, the reader is referred to the web version of this article.)

Then, Floquet-Bloch zero modes of wavenumber $\mathbf{q}$ exist if and only if the linear system

$$C(\mathbf{q})\Phi = \mathbf{0}, \quad \Phi = \begin{bmatrix} \mathbf{u}_1 \\ \mathbf{u}_2 \\ \mathbf{u}_3 \end{bmatrix}, \tag{20}$$

of six equations has a non-trivial solution. The first three equations are automatically satisfied by the ansatz

$$\mathbf{u}_j = \mathbf{U}_o + \varphi_o \bar{\mathbf{x}}_j, \tag{21}$$

where $\mathbf{U}_o$ and φ_o are the new unknowns. The remaining three equations become

$$\begin{bmatrix} (1-Q_1)\mathbf{n}_1' & \langle \mathbf{n}_1, \bar{\mathbf{x}}_3 - Q_1 \bar{\mathbf{x}}_2 \rangle \\ (1-Q_2)\mathbf{n}_2' & \langle \mathbf{n}_2, \bar{\mathbf{x}}_1 - Q_2 \bar{\mathbf{x}}_3 \rangle \\ (1-Q_3)\mathbf{n}_3' & \langle \mathbf{n}_3, \bar{\mathbf{x}}_2 - Q_3 \bar{\mathbf{x}}_1 \rangle \end{bmatrix} \begin{bmatrix} \mathbf{U}_o \\ \varphi_o \end{bmatrix} = \begin{bmatrix} 0 \\ 0 \\ 0 \end{bmatrix} \tag{22}$$

and have a zero-determinant condition equivalent to

$$\prod_j (1-Q_j) \sum_j \langle b_j \mathbf{n}_j, \bar{\mathbf{x}}_{j+1} \rangle + \sum_j (1-Q_{j-1})(1-Q_{j+1}) \langle b_j \mathbf{n}_j, a_j \bar{\mathbf{m}}_j \rangle = 0. \tag{23}$$

From the above equation, it is clear that $\mathbf{q} = \mathbf{0}$, $Q_1 = Q_2 = Q_3 = 1$ provides systematic solutions. These are no other than the periodic zero modes of the previous subsection. For $\mathbf{q} \neq \mathbf{0}$, it can be verified that $Q_j = 1$ (i.e., $\mathbf{q} \perp \mathbf{r}_j$) is a solution if and only if $\mathbf{m}_j$ and $\mathbf{n}_j$ are colinear. No other solutions exist as long as the lattice is not "too distorted" (see Appendix B).

It is then possible to draw the locus of real wavenumbers $\mathbf{q}$ for which Floquet-Bloch zero modes exist. Such a "zero-frequency dispersion diagram" is composed of a number n of straight lines where n is the number of colinear pairs ($\mathbf{m}_j$, $\mathbf{n}_j$). The regular lattice (Fig. 3a) has three pairs of colinear bonds highlighted in blue; thus, its spectrum (Fig. 3e) shows Floquet-Bloch zero modes in the three directions perpendicular to the three lattice vectors $\mathbf{r}_j$. Fig. 3i shows the mode shape of a periodic zero mode ($\mathbf{q} = \mathbf{0}$) and Fig. 3j–l show mode shapes of zero modes with wavenumbers in the directions $\bar{\mathbf{r}}_j$; these mode shapes were previously obtained by Hutchinson and Fleck (2006) and are reproduced here for convenience. Subsequently, distortions that break the alignment of one, two or three pairs of bonds gap one, two or three lines of zero modes, respectively. The resulting lattices and spectra are depicted in Fig. 3b-d and f-h.

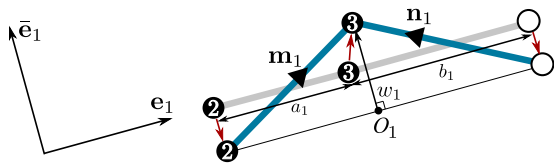

Fig. 4. Illustration of a distortion inducing a regular-distorted phase transition (red arrows): The unmarked node belongs to the boundary of the unit cell and is displaced by the same vector as node 2 so as to maintain periodicity. Elevation w_1 is positive when the vector running from point O_1 to node 3 is in the same direction as $\bar{\mathbf{e}}_1$. The elevations w_j are the only components of the distortion that are relevant here. (For interpretation of the references to colour in this figure legend, the reader is referred to the web version of this article.)

3. Homogenization of Kagome lattices: the microtwist continuum

3.1. Prelude: why Cauchy elasticity is not enough

Having explored Kagome lattices from a purely geometric point of view, it is time to investigate their elastic behavior. We are particularly concerned here with the homogenization limit, i.e., the limit of infinitesimal unit cells. The standard theory of elasticity then permits us to model a Kagome lattice as a homogeneous Cauchy continuum where reigns a stress distribution related to a strain field through Hooke's law

$$\boldsymbol{\sigma} = \mathbf{C}^* : \boldsymbol{\nabla}^s \mathbf{U}, \tag{24}$$

with $\mathbf{C}^*$ being the homogenized fourth-order tensor of effective elastic moduli and $\boldsymbol{\nabla}^s\mathbf{U}$ being the symmetric part of the displacement gradient $\boldsymbol{\nabla}\mathbf{U}$. Interestingly, the overview of zero modes presented in the previous section helps to recognize the limitations of Cauchy's continuum. On one hand, the twisting zero mode in regular lattices produces zero macroscopic strain $\boldsymbol{\nabla}^s\mathbf{U}$ (see, e.g., Fig. 3i) and therefore cannot be accounted for through $\mathbf{U}$ or its gradients. Conversely, a Cauchy's continuum admits no zero modes unless $\mathbf{C}^*$ was singular. By contrast, regular Kagome lattices admit a rich family of zero modes and are known to exhibit a non-singular $\mathbf{C}^*$.

Extrapolating by continuity, we argue that Cauchy's continuum will also be a poor model for weakly-distorted lattices, i.e., lattices where bonds along $\mathbf{m}_j$ and $\mathbf{n}_j$ are close to being colinear. Such lattices necessitate a richer continuum than that of Cauchy for their accurate modeling. In the remainder of this section, we find that continuum.

3.2. Three perturbations

Starting with a regular Kagome lattice, we introduce three perturbations.

First, we induce a regular-distorted phase transition by perturbing the initial positions of the nodes so as to break the alignment of any one of the three pairs $(\mathbf{m}_j, \mathbf{n}_j)$. Letting $(\mathbf{e}_j, \bar{\mathbf{e}}_j)$ be an orthonormal basis colinear to $(\mathbf{r}_j, \bar{\mathbf{r}}_j)$, a weakly-distorted lattice is obtained and is characterized by

$$\mathbf{m}_j = \mathbf{e}_j + \frac{w_j}{a_j}\bar{\mathbf{e}}_j + O\left(\frac{w_j}{a_j}\right)^2, \quad \mathbf{n}_j = -\mathbf{e}_j + \frac{w_j}{b_j}\bar{\mathbf{e}}_j + O\left(\frac{w_j}{b_j}\right)^2, \tag{25}$$

where the parameters w_j control the geometric distortion and are illustrated on Fig. 4.

Second, we assume that the displacements $\mathbf{u}_j^{l,m,n}$ vary slowly with the unit cell indices (l, m, n). That is $\mathbf{u}_j^{l,m,n} = \mathbf{u}_j(\mathbf{x}^{l,m,n})$ where the $\mathbf{u}_j = \mathbf{u}_j(\mathbf{x})$ are now slowly varying fields of the space variable $\mathbf{x}$. More importantly, the leading-order Taylor expansions

$$\begin{aligned}
\mathbf{u}_j^{l+1,m,n} - \mathbf{u}_j^{l,m,n} &= \partial_1 \mathbf{u}_j, \\
\mathbf{u}_j^{l,m+1,n} - \mathbf{u}_j^{l,m,n} &= \partial_2 \mathbf{u}_j, \\
\mathbf{u}_j^{l,m,n+1} - \mathbf{u}_j^{l,m,n} &= \partial_3 \mathbf{u}_j,
\end{aligned} \tag{26}$$

hold with $\partial_j = \langle \mathbf{r}_j, \boldsymbol{\nabla} \rangle$ being the differential with respect to $\mathbf{x}$ in direction $\mathbf{r}_j$. Then, the functions $\mathbf{u}_j$ are slowly varying in space if and only if $\|\partial_j\| \ll 1$, i.e., if and only if their spectrum is dominated by long wavelengths.

Third, we assume that the displacements $\mathbf{u}_j^{l,m,n}$ change with respect to time at low or vanishing angular frequencies ω that satisfy $\omega\sqrt{\max(m_j)} \ll \sqrt{\min(\alpha_j, \beta_j)}$.

Accordingly, in what follows, the behavior of Kagome lattices is investigated in the homogenization limit and, specifically, in the critical regime

$$\|\partial_j\| \sim \sqrt{\frac{\max(m_j)}{\min(\alpha_j, \beta_j)}}\omega \sim \frac{|w_j|}{\min(a_j, b_j)} \ll 1 \tag{27}$$

where all three introduced perturbations are *a priori* of the same order of magnitude.

3.3. Asymptotic expansions

We start by revisiting the equations of the previous section and replace them with their second-order asymptotic expansions. For instance, injecting (25) and (26) back into (2) yields

$$\begin{bmatrix} y_1 \\ y_2 \\ y_3 \\ z_1 \\ z_2 \\ z_3 \end{bmatrix} = C \begin{bmatrix} \mathbf{u}_1 \\ \mathbf{u}_2 \\ \mathbf{u}_3 \end{bmatrix} = C\Phi, \quad C = C_0 + \delta C + \delta^2 C + \dots, \tag{28}$$

where the elongations y_j and z_j, like the displacements $\mathbf{u}_j$, are all functions of the space variable $\mathbf{x}$; C is a differential compatibility operator; C_0 is its restriction to periodic configurations over a regular lattice; and δC and $\delta^2 C$ are its first-order and second-order corrections. We have previously encountered C_0 in Eq. (9); here it specifies into

$$C_0 = \begin{bmatrix} \mathbf{0} & -\mathbf{e}_1' & \mathbf{e}_1' \\ \mathbf{e}_2' & \mathbf{0} & -\mathbf{e}_2' \\ -\mathbf{e}_3' & \mathbf{e}_3' & \mathbf{0} \\ \mathbf{0} & \mathbf{e}_1' & -\mathbf{e}_1' \\ -\mathbf{e}_2' & \mathbf{0} & \mathbf{e}_2' \\ \mathbf{e}_3' & -\mathbf{e}_3' & \mathbf{0} \end{bmatrix}. \tag{29}$$

As for the correction $\delta C = \delta_w C + \delta_x C$, it is composed of two terms, the first of which is due to the perturbation that induces the regular-distorted phase transition, namely

$$\delta_w C = \begin{bmatrix} \mathbf{0} & -w_1\bar{\mathbf{e}}_1'/a_1 & w_1\bar{\mathbf{e}}_1'/a_1 \\ w_2\bar{\mathbf{e}}_2'/a_2 & \mathbf{0} & -w_2\bar{\mathbf{e}}_2'/a_2 \\ -w_3\bar{\mathbf{e}}_3'/a_3 & w_3\bar{\mathbf{e}}_3'/a_3 & \mathbf{0} \\ \mathbf{0} & -w_1\bar{\mathbf{e}}_1'/b_1 & w_1\bar{\mathbf{e}}_1'/b_1 \\ w_2\bar{\mathbf{e}}_2'/b_2 & \mathbf{0} & -w_2\bar{\mathbf{e}}_2'/b_2 \\ -w_3\bar{\mathbf{e}}_3'/b_3 & w_3\bar{\mathbf{e}}_3'/b_3 & \mathbf{0} \end{bmatrix}, \tag{30}$$

and the second of which is due to the fields being slowly varying in space, namely

$$\delta_x C = \begin{bmatrix} \mathbf{0} & \mathbf{0} & \mathbf{0} \\ \mathbf{0} & \mathbf{0} & \mathbf{0} \\ \mathbf{0} & \mathbf{0} & \mathbf{0} \\ \mathbf{0} & \mathbf{e}_1'\partial_1 & \mathbf{0} \\ \mathbf{0} & \mathbf{0} & \mathbf{e}_2'\partial_2 \\ \mathbf{e}_3'\partial_3 & \mathbf{0} & \mathbf{0} \end{bmatrix}. \tag{31}$$

Lastly, the entries of the second-order correction $\delta^2 C$ will not be calculated as they turn out to be of no use for our purposes.

Similarly, displacements can be Taylor-expanded:

$$\Phi = \Phi_0 + \delta\Phi + \delta^2\Phi + \dots, \quad \Phi = \begin{bmatrix} \mathbf{u}_1 \\ \mathbf{u}_2 \\ \mathbf{u}_3 \end{bmatrix}, \tag{32}$$

where Φ_0 gathers the leading-order displacements, $\delta\Phi$ their first-order corrections and so on, and all are functions of $\mathbf{x}$. As for the motion equation, it reads

$$-C'KC\Phi + F = -\omega^2 M\Phi, \tag{33}$$

where $K = \mathrm{diag}(\alpha_1, \alpha_2, \alpha_3, \beta_1, \beta_2, \beta_3)$ and $M = \mathrm{diag}(m_1\mathbf{I}, m_2\mathbf{I}, m_3\mathbf{I})$ are the diagonal rigidity and mass matrices and where C' is the adjoint operator of C obtained by transposing C and mapping ∂_j to $-\partial_j$. As for F, it corresponds to body force and is taken to be slowly varying in space and of the same order of magnitude as inertial forces. In the following, we derive an equation that governs the leading-order displacements Φ_0 thus interpreted as the macroscopic motion equation. But first, the motion equation must be solved to leading and first orders.

3.4. Leading and first order auxiliary problems

Keeping only leading-order terms in the motion Eq. (33) yields

$$-C_0'KC_0\Phi_0 = 0. \tag{34}$$

Therefore, $\Phi_0'C_0'KC_0\Phi_0 = 0$ and, by definiteness of K, $C_0\Phi_0 = 0$. We have seen in Section 2.3 that the solutions to this equation are translation and twisting motions so that there exist slowly varying vector and scalar fields, $\mathbf{U} = \mathbf{U}(\mathbf{x})$ and $\varphi = \varphi(\mathbf{x})$, such that

$$\Phi_0 = D\mathbf{U} + T\varphi. \tag{35}$$

Then, keeping only the first-order terms entails

$$-C_0'KC_0\delta\Phi+\Psi=0,\quad \Psi=-C_0'K(\delta_wC+\delta_xC)(D\mathbf{U}+T\varphi). \tag{36}$$

Thus, $\delta\Phi$ appears as a solution to a forced motion equation. Matrix C_0 being singular, the above equation admits solutions if and only if Ψ is balanced in the sense of being orthogonal to all zero modes:

$$D'\Psi=0,\quad T'\Psi=0. \tag{37}$$

Alternatively, Ψ is balanced if and only if it belongs to the range of matrix C_0', which in turn is identical to the range of matrix

$$G=\begin{bmatrix}G_1 & G_2 & G_3\end{bmatrix},\quad G_1=\begin{bmatrix}\mathbf{0}\\-\mathbf{e}_1\\\mathbf{e}_1\end{bmatrix},\quad G_2=\begin{bmatrix}\mathbf{e}_2\\\mathbf{0}\\-\mathbf{e}_2\end{bmatrix},\quad G_3=\begin{bmatrix}-\mathbf{e}_3\\\mathbf{e}_3\\\mathbf{0}\end{bmatrix}, \tag{38}$$

given that $C_0'=\begin{bmatrix}G & -G\end{bmatrix}$. That is, Ψ is a balanced loading if and only if it reads

$$\Psi=G\psi,\quad \psi=\begin{bmatrix}\psi_1\\\psi_2\\\psi_3\end{bmatrix}, \tag{39}$$

where the ψ_j are the generalized coordinates of Ψ along the G_j. In Eq. (36), Ψ is indeed balanced because it is pre-multiplied by C_0'. A straightforward calculation then shows that

$$\psi=\begin{bmatrix}(\gamma\beta_1-\alpha_1)w_1\\(\gamma\beta_2-\alpha_2)w_2\\(\gamma\beta_3-\alpha_3)w_3\end{bmatrix}\varphi+\frac{1}{3}\begin{bmatrix}\beta_1h_1\partial_1\\\beta_2h_2\partial_2\\\beta_3h_3\partial_3\end{bmatrix}\varphi+\begin{bmatrix}\beta_1\langle\mathbf{e}_1,\partial_1\rangle\\\beta_2\langle\mathbf{e}_2,\partial_2\rangle\\\beta_3\langle\mathbf{e}_3,\partial_3\rangle\end{bmatrix}\mathbf{U}, \tag{40}$$

where $\gamma=a_j/b_j$ is the j-independent similarity ratio and $h_j=\langle\mathbf{e}_j,a_{j-1}\bar{\mathbf{e}}_{j-1}\rangle$ is the height of node j in the triangle whose vertices are nodes 1, 2 and 3 previously called triangle Δ.

Therefore, a solution $\delta\Phi$ exists and is given by

$$\delta\Phi=\Gamma\psi,\quad \Gamma=\begin{bmatrix}\Gamma_1 & \Gamma_2 & \Gamma_3\end{bmatrix}, \tag{41}$$

where Γ_j is a solution to

$$-C_0'KC_0\Gamma_j+G_j=0. \tag{42}$$

The Γ_j are straightforward to determine from the above equation, first by solving for $KC_0\Gamma_j$, then for $C_0\Gamma_j$ and finally for Γ_j. Also, note that it is enough to calculate Γ_1 since Γ_2 and Γ_3 can be deduced by permutation symmetry. Skipping these steps, it comes that

$$\Gamma=-\frac{1}{2}\begin{bmatrix}\mathbf{0} & \frac{a_3/h_2}{\alpha_2+\beta_2}\bar{\mathbf{e}}_3 & \frac{a_2/h_3}{\alpha_3+\beta_3}\bar{\mathbf{e}}_2\\ \frac{a_3/h_1}{\alpha_1+\beta_1}\bar{\mathbf{e}}_3 & \mathbf{0} & \frac{a_1/h_3}{\alpha_3+\beta_3}\bar{\mathbf{e}}_1\\ \frac{a_2/h_1}{\alpha_1+\beta_1}\bar{\mathbf{e}}_2 & \frac{a_1/h_2}{\alpha_2+\beta_2}\bar{\mathbf{e}}_1 & \mathbf{0}\end{bmatrix}. \tag{43}$$

It is worth mentioning that the determined solution $\delta\Phi$ is not unique and can be modified by addition of an arbitrary correction $D\delta\mathbf{U}+T\delta\varphi$. However, this will have no influence on what follows.

3.5. Macroscopic equations of motion

Keeping the second-order terms in the motion equation yields

$$\begin{aligned}&-C_0'KC_0\delta^2\Phi-C_0'K(\delta_wC+\delta_xC)\delta\Phi-(\delta_wC+\delta_xC)'KC_0\delta\Phi\\&-C_0'K\delta^2C\Phi_0-(\delta_wC+\delta_xC)'K(\delta_wC+\delta_xC)\Phi_0+F=-\omega^2M\Phi_0.\end{aligned} \tag{44}$$

Thus, $\delta^2\Phi$, just like $\delta\Phi$ before, is a solution to a forced motion equation and exists if and only if the orthogonality conditions (37) are enforced. These are derived by multiplying Eq. (44) by D' and by T' and read

$$-D'(\delta_xC)'KC_0\delta\Phi-D'(\delta_xC)'K(\delta_wC+\delta_xC)\Phi_0+D'F=-\omega^2D'M\Phi_0, \tag{45}$$

and

$$-T'(\delta_wC+\delta_xC)'KC_0\delta\Phi-T'(\delta_wC+\delta_xC)'K(\delta_wC+\delta_xC)\Phi_0+T'F=-\omega^2T'M\Phi_0. \tag{46}$$

Therein, the unknown term $C_0'KC_0\delta^2\Phi$ vanishes as it is pre-multiplied by C_0'. Thanks to the expression of $\delta\Phi$ given by Eqs. (40) and (41), we see that the above two equations involve the leading-order displacements spanned by $\mathbf{U}$ and φ and the applied body force F, exclusively. Accordingly, they can be interpreted as a pair of macroscopic motion equations governing the macroscopic DOFs $\mathbf{U}$ and φ. Next, we write these equations in a form more suitable for interpretation, extract appropriate measures of strain and stress and reveal the constitutive law that relates them.

3.6. Microtwist continuum

The quantities involved in (45) and (46) can be fully evaluated simply by injecting therein the derived expressions (11), (12), (29), (30), (31), (40) and (43). As a result, the macroscopic motion equations can be recast into the form

$$\begin{aligned} -\omega^2(\rho\mathbf{U}+\rho\bar{\mathbf{d}}\varphi) &= \mathbf{F}+\nabla\cdot\left(\mathbf{C}:\nabla^s\mathbf{U}+\mathbf{B}\cdot\nabla\varphi+\mathbf{M}\varphi\right),\\ -\omega^2(\rho\langle\bar{\mathbf{d}},\mathbf{U}\rangle+\eta\varphi) &= \tau+\nabla\cdot\left(\mathbf{B}:\nabla^s\mathbf{U}+\mathbf{D}\cdot\nabla\varphi+\mathbf{A}\varphi\right)\\ &\quad -\mathbf{M}:\nabla^s\mathbf{U}-\mathbf{A}\cdot\nabla\varphi-L\varphi, \end{aligned} \tag{47}$$

where $\nabla^s\mathbf{U}$ is the symmetric part of the macroscopic displacement gradient, $\nabla\varphi$ is the twisting gradient, the operators $\cdot$ and : symbolize simple and double contraction of tensors and $\nabla\cdot$ is the divergence operator.

Vector $\mathbf{d}=\sum_j m_j\mathbf{x}_j/\sum_j m_j$ is the position vector of the center of mass of triangle Δ with respect to its geometric center and ρ and η are mass density and moment of inertia density

$$\rho=\frac{\gamma^2}{ah(1+\gamma)^2}\sum_j m_j,\quad \eta=\frac{\gamma^2}{ah(1+\gamma)^2}\sum_j m_j\left\|\mathbf{x}_j\right\|^2, \tag{48}$$

where $ah/2\equiv a_jh_j/2$ is the area of triangle Δ and $ah(1+\gamma)^2/\gamma^2$ is the area of a unit cell and both are independent of j.

The vector-scalar pair $(\mathbf{F},\tau)$ is the resultant force-torque acting on a unit cell per unit cell area with respect to the geometric center of triangle Δ. Its components read

$$\mathbf{F}=\frac{\gamma^2}{ah(1+\gamma)^2}\sum_j\mathbf{f}_j,\quad \tau=\frac{\gamma^2}{ah(1+\gamma)^2}\sum_j\langle\bar{\mathbf{x}}_j,\mathbf{f}_j\rangle. \tag{49}$$

The involved effective tensors are given by

$$\begin{aligned} &\mathbf{C}=\sum_j\frac{a_j}{h_j}k_j\mathbf{e}_{jjjj},\quad \mathbf{B}=\frac{1}{3}\sum_j a_jk_j\mathbf{e}_{jjj},\quad \mathbf{M}=\gamma\sum_j\frac{w_j}{h_j}k_j\mathbf{e}_{jj},\\ &\mathbf{D}=\frac{ah}{9}\sum_j k_j\mathbf{e}_{jj},\quad \mathbf{A}=\frac{\gamma}{3}\sum_j w_jk_j\mathbf{e}_j,\quad L=\frac{\gamma^2}{ah}\sum_j w_j^2k_j, \end{aligned} \tag{50}$$

where $\mathbf{e}_{jjjj}$, $\mathbf{e}_{jjj}$ and $\mathbf{e}_{jj}$ are the fourth, third and second tensorial powers of $\mathbf{e}_j$ respectively, and $k_j=\alpha_j\beta_j/(\alpha_j+\beta_j)$. Accordingly, the above effective tensors are completely symmetric tensors of order four ($\mathbf{C}$), three ($\mathbf{B}$), two ($\mathbf{M}$, $\mathbf{D}$), one ($\mathbf{A}$) and zero (L).

Alternatively, the macroscopic motion equations can be written as the balance equations

$$-\omega^2(\rho\mathbf{U}+\rho\bar{\mathbf{d}}\varphi)=\mathbf{F}+\nabla\cdot\boldsymbol{\sigma},\quad -\omega^2(\rho\langle\bar{\mathbf{d}},\mathbf{U}\rangle+\eta\varphi)=\tau+\nabla\cdot\boldsymbol{\xi}+s, \tag{51}$$

where $\boldsymbol{\sigma}$, $\boldsymbol{\xi}$ and s are second, first and zero-order tensorial stress measures related to the strain measures $\nabla^s\mathbf{U}$, $\nabla\varphi$ and φ through the macroscopic constitutive law

$$\begin{bmatrix}\boldsymbol{\sigma}\\ \boldsymbol{\xi}\\ -s\end{bmatrix}=\begin{bmatrix}\mathbf{C}&\mathbf{B}&\mathbf{M}\\ \mathbf{B}&\mathbf{D}&\mathbf{A}\\ \mathbf{M}&\mathbf{A}&L\end{bmatrix}\begin{bmatrix}\nabla^s\mathbf{U}\\ \nabla\varphi\\ \varphi\end{bmatrix}. \tag{52}$$

With the help of the divergence theorem, the motion equations can further be integrated over any domain Ω with boundary $\partial\Omega$ and outward unit normal $\mathbf{N}$ to yield Euler's laws

$$\begin{aligned} -\omega^2\int_\Omega\left(\rho\mathbf{U}+\rho\bar{\mathbf{d}}\varphi\right) &= \int_\Omega\mathbf{F}+\int_{\partial\Omega}\boldsymbol{\sigma}\cdot\mathbf{N},\\ -\omega^2\int_\Omega\left(\rho\langle\bar{\mathbf{d}},\mathbf{U}\rangle+\eta\varphi\right) &= \int_\Omega\tau+\int_{\partial\Omega}\langle\boldsymbol{\xi},\mathbf{N}\rangle+\int_\Omega s. \end{aligned} \tag{53}$$

Knowing that $(\mathbf{F},\tau)$ is the resultant force-torque, the above equations readily provide an interpretation of the stress measures: $\boldsymbol{\sigma}$ is *Cauchy's stress* whereby $\boldsymbol{\sigma}\cdot\mathbf{N}$ yields the stress vector applied to a length element of normal $\mathbf{N}$; $\boldsymbol{\xi}$ is *couple stress* whereby $\langle\boldsymbol{\xi},\mathbf{N}\rangle$ yields the torque per unit length applied to a length element of normal $\mathbf{N}$; and s is a *hyperstress* counteracting the external body torque τ.

We thus complete the description of the behavior of a general regular or weakly-distorted Kagome lattice, in the homogenization limit, as an enriched continuum with an extra DOF and additional measures of strain, stress and inertia. This enriched continuum is baptized *the microtwist continuum*.

3.7. Discussion

In conclusion of this section, several points are worth stressing. We do so in the following somewhat lengthy discussion.

1. As it has more DOFs than dimensions, the microtwist medium qualifies as an enriched continuum in the sense of generalized continua (Eringen, 1999; Mindlin, 1964). The microtwist medium can be understood as a particular Cosserat medium where the microrotation DOF φ^{mr} and infinitesimal rotation $\boldsymbol{\nabla}\times\mathbf{U}/2$ only appear in the combination $\varphi=\varphi^{\mathrm{mr}}-\boldsymbol{\nabla}\times\mathbf{U}/2$. Such a Cosserat medium would be unusual however as it would involve the second gradient of $\mathbf{U}$, specifically $\boldsymbol{\nabla}(\boldsymbol{\nabla}\times\mathbf{U})$, through $\boldsymbol{\nabla}\varphi$. This brings unnecessary formal complications; it seems then that Kagome lattices are more naturally understood as their own microtwist media. Microtwist media are also isomorphic to a subclass of Eringen's micromorphic media where microdeformation is restricted to a one dimensional space. Some refer to such a medium as a microdilatation medium; see, e.g., Forest and Sievert (2006).
2. In the preceding derivations, nodes were assumed to behave like perfect hinges. The consequence is that variations of angles between the bonds meeting at a given node cost no elastic energy at all. It could be of interest however to inspect the mechanics of Kagome lattices with elastic hinges as they are expected to be better models of real structures. Taking the influence of elasticity in the hinges turns out to be remarkably simple so long as the hinges are soft. Indeed, in that case, it is enough to change the expression of the effective parameter L into
$$L=\kappa+\frac{\gamma^2}{ah}\sum_j w_j^2 k_j \tag{54}$$
where κ is an effective torsional spring constant function of geometry and of the elasticity moduli of the hinges. A proof is outlined in Appendix C.
3. The quadratic form of strain energy density ϵ is
$$\epsilon=\frac{\boldsymbol{\sigma}:\boldsymbol{\nabla}^s\mathbf{U}+\boldsymbol{\xi}\cdot\boldsymbol{\nabla}\varphi-s\varphi}{2}, \tag{55}$$
where stresses are linear combinations of strains following the constitutive law of the microtwist continuum. Skipping calculations, its expression can be recast into
$$\epsilon=\sum_j\frac{k_j}{2ah}\left(a_j\mathbf{e}_{jj}:\boldsymbol{\nabla}^s\mathbf{U}+\frac{ah}{3}\mathbf{e}_j\cdot\boldsymbol{\nabla}\varphi+\gamma w_j\varphi\right)^2+\frac{\kappa}{2}\varphi^2 \tag{56}$$
where it is clear that it is non-negative. Definiteness however completely relies on the elastic constants k_j and κ being non-null. In particular, when the hinges are perfect ($\kappa=0$), strain energy is semi-definite and therefore allows for microstructural zero modes to manifest on the macroscopic scale.

4. Microtwist elasticity and Cauchy's elasticty

In this section, we draw a quantitative comparison between Cauchy's and microtwist elasticity in the context of low-frequency wave propagation and dispersion. But first, the governing equations of the relevant effective continua are exemplified for a family of equilateral Kagome lattices.

4.1. Model reduction to Cauchy's continuum

Hutchinson and Fleck (2006), among others, developed a homogenization theory for a few Kagome lattices and other periodic trusses based on a kinematic hypothesis known as the Cauchy-Born hypothesis. It states that the displacements are the sum of one linear and one periodic field
$$\mathbf{u}_j^{l,m,n}=\boldsymbol{\varepsilon}\cdot\mathbf{x}_j^{l,m,n}+\mathbf{u}_j, \tag{57}$$
the linear part being the result of an imposed uniform macroscopic deformation $\boldsymbol{\varepsilon}$. In doing so, they neglected[3] the contribution of the twisting gradient $\boldsymbol{\nabla}\varphi$ to strain energy as well as the presence of any dynamics. Our model reduces to theirs when these approximations are implemented.

As a matter of fact, strain energy density ϵ, with twisting gradients neglected, simplifies into
$$\epsilon^*=\frac{1}{2}\boldsymbol{\nabla}^s\mathbf{U}:\mathbf{C}:\boldsymbol{\nabla}^s\mathbf{U}+\mathbf{M}:\boldsymbol{\nabla}^s\mathbf{U}\varphi+\frac{1}{2}L\varphi^2. \tag{58}$$
Hence, the static Lagrangian $\int_\Omega\epsilon^*-\langle\mathbf{F},\mathbf{U}\rangle$ of a domain Ω in the absence of body torques τ is minimal for
$$\varphi=-\frac{\mathbf{M}:\boldsymbol{\nabla}^s\mathbf{U}}{L},\quad L\neq 0. \tag{59}$$
Thus, under these assumptions, φ is no longer a free variable (i.e., a DOF) and is dictated pointwise by the value of the macroscopic strain $\boldsymbol{\nabla}^s\mathbf{U}$. Substituting for φ, we obtain a reduced strain energy density in the form
$$\epsilon^*=\frac{1}{2}\boldsymbol{\nabla}^s\mathbf{U}:\mathbf{C}^*:\boldsymbol{\nabla}^s\mathbf{U},\quad \mathbf{C}^*=\mathbf{C}-\frac{1}{L}\mathbf{M}\otimes\mathbf{M}, \tag{60}$$

[3] We stress that Hutchinson and Fleck (2006) were aware of the limitations of their model; see the first footnote of their paper.

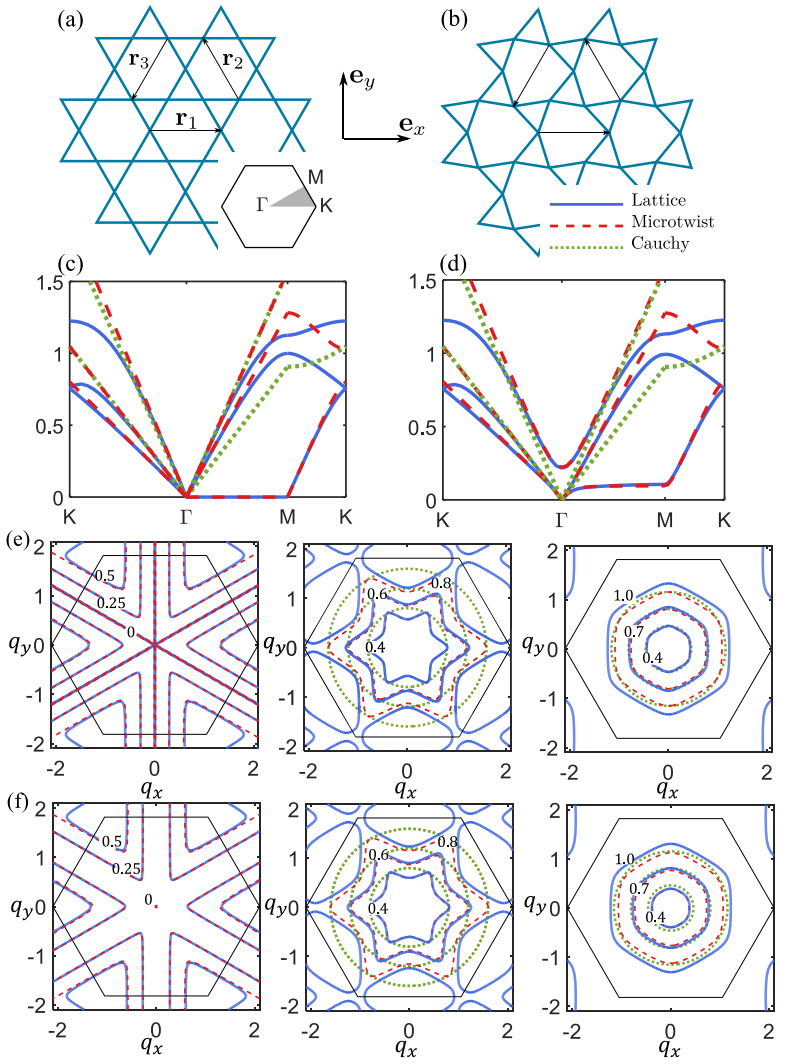

Fig. 5. Two equilateral Kagome lattices and their dispersion diagrams: (a) a regular lattice; (b) a pre-twisted (distorted) lattice; (c, d) their respective dispersion diagrams; (e, f) their respective isofrequency contours: left, middle and right correspond to the first, second and third dispersion surfaces. The used numerical values are: $a_j = b_j = 1$ and $\alpha_j = \beta_j = 1$; $w_j = 0$ for (a); and $w_j/a_j \approx -4\%$ for (b).

with a reduced Hooke's law $\boldsymbol{\sigma} = \mathbf{C}^* : \boldsymbol{\nabla}^s\mathbf{U}$. Note that for Kagome lattices with $L = 0$, we also have $\mathbf{M} = \mathbf{0}$ by Eq. (50). In that case, ϵ^* becomes independent of φ and we readily obtain $\mathbf{C}^* = \mathbf{C}$. These expressions of $\mathbf{C}^*$ are in agreement with, and generalize, the results of Hutchinson and Fleck (2006) to arbitrary regular and weakly-distorted Kagome lattices.

Using the reduced Hooke's law is appealing as it is significantly simpler than the microtwist constitutive law. Nonetheless, neglecting the twisting gradient $\boldsymbol{\nabla}\varphi$ cannot be justified except in the presence of static uniform fields. Taking the contributions of twisting gradients to strain energy into account, specifically through the effective tensors (**B, D, A**), will in fact greatly improve the quality of the predictions of the effective medium theory; various quantitative demonstrations are suggested in the remainder of the paper.

4.2. Example: equilateral lattices

We readily exemplify the equations of microtwist and Cauchy's elasticity in the case of Kagome lattices whose all edges are equal in length. We call such lattices *equilateral*; see Fig. 5a, b. We further suppose that equilateral lattices possess perfect hinges, j-independent parameters and a similarity ratio $\gamma = 1$. Such lattices are therefore invariant by rotations of

order 3. Consequently, their effective tensors **C, D** and **M** are isotropic.[4] Specifically, they are given by

$$\mathbf{C} : \nabla^s \mathbf{U} = \mu(2\nabla^s \mathbf{U} + \mathrm{tr}(\nabla^s \mathbf{U})\mathbf{I}), \quad \mathbf{D} = \frac{a^2}{3}\mu \mathbf{I}, \quad \mathbf{M} = 4\frac{w}{a}\mu \mathbf{I}, \tag{61}$$

with $\mu = \sqrt{3}k/4$. In addition, $L = 8w^2\mu/a^2$ whereas vector $\mathbf{A}$ and the inertial coupling $\bar{\mathbf{d}}$ vanish. As for mass and moment of inertia densities, they simplify into

$$\rho = \frac{\sqrt{3}m}{2a^2}, \quad \eta = \frac{m}{2\sqrt{3}}. \tag{62}$$

Last, the third-order effective tensor $\mathbf{B}$ is anisotropic. Its components depend on the chosen basis. In a basis $(\mathbf{e}_x, \mathbf{e}_y)$ aligned with $(\mathbf{e}_1, \bar{\mathbf{e}}_1)$, its components take the form

$$B_{xxx} = -B_{xyy} = -B_{yxy} = -B_{yyx} = \frac{a}{\sqrt{3}}\mu, \quad B_{yxx} = B_{xyx} = B_{xxy} = B_{yyy} = 0. \tag{63}$$

These results are in agreement with the strain energy density postulated by Sun et al. (2012).

By the same logic as above, the elasticity tensor $\mathbf{C}^*$ of the reduced Hooke's law is isotropic. Its expression depends on whether the lattice is distorted ($w \neq 0$) or regular ($w = 0$). For a distorted lattice, application of Eq. (60) leads to

$$\mathbf{C}^* : \nabla^s \mathbf{U} = \mu(2\nabla^s \mathbf{U} - \mathrm{tr}(\nabla^s \mathbf{U})\mathbf{I}), \tag{64}$$

with a Young's modulus $E = 0$ and a Poisson's coefficient $\nu = -1$. For a regular lattice, $\mathbf{C}^* = \mathbf{C}$ exhibits a Young's modulus $E = 8\mu/3$ and a Poisson's coefficient $\nu = 1/3$; see also Lubensky et al. (2015).

Last, with these expressions, the motion equations of the microtwist continuum can be fully expanded into

$$\begin{aligned}
-\omega^2 \frac{\rho}{\mu} U_x &= 3U_{x,xx} + 2U_{y,xy} + U_{x,yy} + \frac{a}{\sqrt{3}}(\varphi_{,xx} - \varphi_{,yy}) + 4\frac{w}{a}\varphi_{,x}, \\
-\omega^2 \frac{\rho}{\mu} U_y &= 3U_{y,yy} + 2U_{x,xy} + U_{y,xx} - \frac{2a}{\sqrt{3}}\varphi_{,xy} + 4\frac{w}{a}\varphi_{,y}, \\
-\omega^2 \frac{\eta}{\mu} \varphi &= \frac{a}{\sqrt{3}}(U_{x,xx} - 2U_{y,xy} - U_{x,yy}) + \frac{a^2}{3}(\varphi_{,xx} + \varphi_{,yy}) \\
&\quad -4\frac{w}{a}(U_{x,x} + U_{y,y}) - 8\frac{w^2}{a^2}\varphi,
\end{aligned} \tag{65}$$

where a comma denotes a partial derivative with respect to the relevant space coordinates. This set of equations can be solved by prescribing appropriate boundary conditions where either $\mathbf{U}$, φ, $\boldsymbol{\sigma} \cdot \mathbf{N}$ or $\langle \boldsymbol{\xi}, \mathbf{N} \rangle$, or a combination thereof is given, using the finite element method for instance.

4.3. Dispersion diagrams

Free harmonic plane waves propagated through the bulk of a Kagome lattice exist at specific frequencies ω and wavenumbers $\mathbf{q}$ solution to the dispersion relation

$$\det\left(C(\mathbf{q})' K C(\mathbf{q}) - \omega^2 M\right) = 0. \tag{66}$$

The Kagome lattice having six DOFs per unit cell, there exists six solution frequencies $\omega = \omega_d(\mathbf{q})$, $d = 1, 2, \ldots 6$, for any given wavenumber $\mathbf{q}$. The microtwist continuum, having three DOFs per unit cell, will be able, at best, to account for the lowest three of them $\omega = \tilde{\omega}_d(\mathbf{q})$, $d = 1, 2, 3$. These frequencies are obtained by injecting

$$\mathbf{U}(\mathbf{x}, t) = \mathbf{U}_o \exp(i\langle \mathbf{q}, \mathbf{x} \rangle), \quad \varphi(\mathbf{x}, t) = \varphi_o \exp(i\langle \mathbf{q}, \mathbf{x} \rangle), \tag{67}$$

in Eq. (47) under zero loading and solving the resulting dispersion relation

$$\det\left(\begin{bmatrix} \mathbf{q}\cdot\mathbf{C}\cdot\mathbf{q} & \mathbf{q}\cdot\mathbf{B}\cdot\mathbf{q} - i\mathbf{q}\cdot\mathbf{M} \\ (\mathbf{q}\cdot\mathbf{B}\cdot\mathbf{q} - i\mathbf{q}\cdot\mathbf{M})' & \mathbf{q}\cdot\mathbf{D}\cdot\mathbf{q} + L \end{bmatrix} - \omega^2\rho \begin{bmatrix} \mathbf{I} & \bar{\mathbf{d}} \\ \bar{\mathbf{d}}' & \eta/\rho \end{bmatrix}\right) = 0. \tag{68}$$

Hereafter we draw a comparison between the two, discrete and microtwist, models. For reference, we also include the dispersion diagrams of the effective Cauchy continuum.

Thus let us consider the two previously introduced equilateral Kagome lattices of Fig. 5a and b. Plots (c) and (d) of their dispersion diagrams show satisfactory agreement between the discrete and microtwist models up to frequencies comparable to the cutoff frequencies of the three lowest dispersion branches and that for small to medium wavenumbers. By contrast, the Cauchy model systematically misses one dispersion branch, namely the one corresponding to the twisting motion, and in some directions, e.g., ΓM direction, significantly underestimates the shear acoustic branch. These observations hold for the isofrequency contours shown on plots (e) and (f). Note again how the Cauchy model completely omits the first dispersion

[4] In 2D, tensors of order 2 and 4 are isotropic, i.e., invariant by proper plane rotations, as soon as they are invariant by rotations of order 3.

surface (left); in particular, it exhibits no traces of the zero modes of the regular lattice. The Cauchy model does well in particular highly symmetric directions over the second dispersion surface (middle) and is satisfactory overall for the third surface (right). However, the Cauchy model fails to describe the directional, i.e., anisotropic, behavior of the second dispersion surface. By contrast, the microtwist model appears consistently accurate across all three surfaces for wavelengths as small as two unit cells. In conclusion of this section, we highlight that by correcting Cauchy's model, microtwist elasticity should help improve the accuracy of ultrasound-based evaluation techniques for lattice-based materials whereby the elastic properties are inferred from wave speed measurements.

5. Elastic and topological polarization

5.1. Parity symmetry in microtwist elasticity

Consider a homogeneous centrosymmetric domain Ω, i.e., such that $\mathbf{x} \in \Omega$ implies $-\mathbf{x} \in \Omega$. Suppose Ω obeys Cauchy's theory of elasticity and let $\mathbf{U}(\mathbf{x})$ be a displacement field in static equilibrium so that

$$\boldsymbol{\nabla} \cdot (\mathbf{C}^* : \boldsymbol{\nabla}^s \mathbf{U}(\mathbf{x})) = \mathbf{0}. \tag{69}$$

Now let $\mathbf{V}(\mathbf{x})$ be another displacement field deduced from $\mathbf{U}(\mathbf{x})$ by the space inversion $\mathbf{V}(\mathbf{x}) = \mathbf{U}(-\mathbf{x})$. Then, thanks to the chain rule $\boldsymbol{\nabla}^s \mathbf{V}(\mathbf{x}) = -\boldsymbol{\nabla}^s \mathbf{U}(-\mathbf{x})$, it is straightforward to see that $\mathbf{V}(\mathbf{x})$ is in static equilibrium as well:

$$\boldsymbol{\nabla} \cdot (\mathbf{C}^* : \boldsymbol{\nabla}^s \mathbf{V}(\mathbf{x})) = \mathbf{0}. \tag{70}$$

This symmetry is characteristic of Cauchy's theory of elasticity; it states that the space of solutions is invariant under the space inversion $\mathbf{x} \mapsto -\mathbf{x}$. We will refer to it as Parity (P) symmetry.

Formally, P-symmetry is equivalent to the strain energy density ϵ being an even function of the gradient operator $\boldsymbol{\nabla}$. That is, the formal substitution $\boldsymbol{\nabla} \mapsto -\boldsymbol{\nabla}$ induced by the chain rule leaves the strain energy density as is. While this property holds for Cauchy's strain energy density ϵ^* of Eq. (60), it fails, in general, for the microtwist strain energy density ϵ of Eq. (56). For reference, we have

$$\begin{aligned}
\epsilon(\boldsymbol{\nabla}) &= \sum_j \frac{k_j}{2ah} \left(a_j \mathbf{e}_{jj} : \boldsymbol{\nabla}^s \mathbf{U} + \frac{ah}{3} \mathbf{e}_j \cdot \boldsymbol{\nabla}\varphi + \gamma w_j \varphi \right)^2 + \frac{\kappa}{2}\varphi^2, \\
\epsilon(-\boldsymbol{\nabla}) &= \sum_j \frac{k_j}{2ah} \left(a_j \mathbf{e}_{jj} : \boldsymbol{\nabla}^s \mathbf{U} + \frac{ah}{3} \mathbf{e}_j \cdot \boldsymbol{\nabla}\varphi - \gamma w_j \varphi \right)^2 + \frac{\kappa}{2}\varphi^2.
\end{aligned} \tag{71}$$

Therefore, in the microtwist theory, a Kagome lattice is P-symmetric if and only if all w_j vanish, i.e., if and only if the lattice is regular. Conversely, all distorted lattices, i.e., with at least one non-zero w_j, are P-asymmetric. We will refer to P-asymmetric lattices as *polarized*.

Intuitively, in a polarized lattice, gradients will prefer to point towards specific directions (e.g., left or right, up or down). Indeed, flipping the sign of the gradients can drastically change the strain energy density ϵ. By contrast, P-symmetric lattices are only sensitive to the magnitude of the gradients and not to the direction in which the fields grow or decay. It is paramount to stress here that P-symmetry is different from and independent of material symmetry and the related notions of isotropy or anisotropy. For instance, we have seen that regular equilateral Kagome lattices exhibit a non-zero third order effective constitutive tensor $\mathbf{B}$ which breaks the material centrosymmetry of the constitutive law. Nonetheless, as we have just pointed out, regular lattices are P-symmetric.

In fact, observe how the rule $\boldsymbol{\nabla} \mapsto -\boldsymbol{\nabla}$ acts in the same manner as the rule $w_j \mapsto -w_j$ on the strain energy density ϵ.[5] This means that the effective constitutive tensors responsible for P-asymmetry are the ones that are odd functions of the w_j. We conclude that the tensors $\mathbf{A}$ and $\mathbf{M}$, and not $\mathbf{B}$, are at the origin of macroscopic polarization effects in Kagome lattices. Moreover, tensor $\mathbf{M}$ is alone responsible for polarization effects in the bulk. Indeed, in ϵ, tensor $\mathbf{A}$ only appears in the combination $\boldsymbol{\nabla} \cdot (\mathbf{A}\varphi) - \mathbf{A} \cdot \boldsymbol{\nabla}\varphi$ which vanishes identically. In any case however, both $\mathbf{M}$ and $\mathbf{A}$ contribute to polarization near interfaces or edges since they would be involved in writing the corresponding continuity and boundary conditions weighing on $\boldsymbol{\sigma}$ and $\boldsymbol{\xi}$.

In the remainder of this section, we explore how polarization manifests in the biased way in which zero modes localize near boundaries and investigate the influence this bias has on the elastic response.

5.2. The zero modes of the microtwist continuum

Zero modes, over a continuum, can be reasonably defined as configurations producing zero stress measures:

$$\boldsymbol{\sigma} = \mathbf{0}, \quad \boldsymbol{\xi} = \mathbf{0}, \quad s = 0. \tag{72}$$

[5] This is similar to how in certain physical systems, P-symmetry breaks but CP-symmetry survives where "C" stands for charge conjugation.

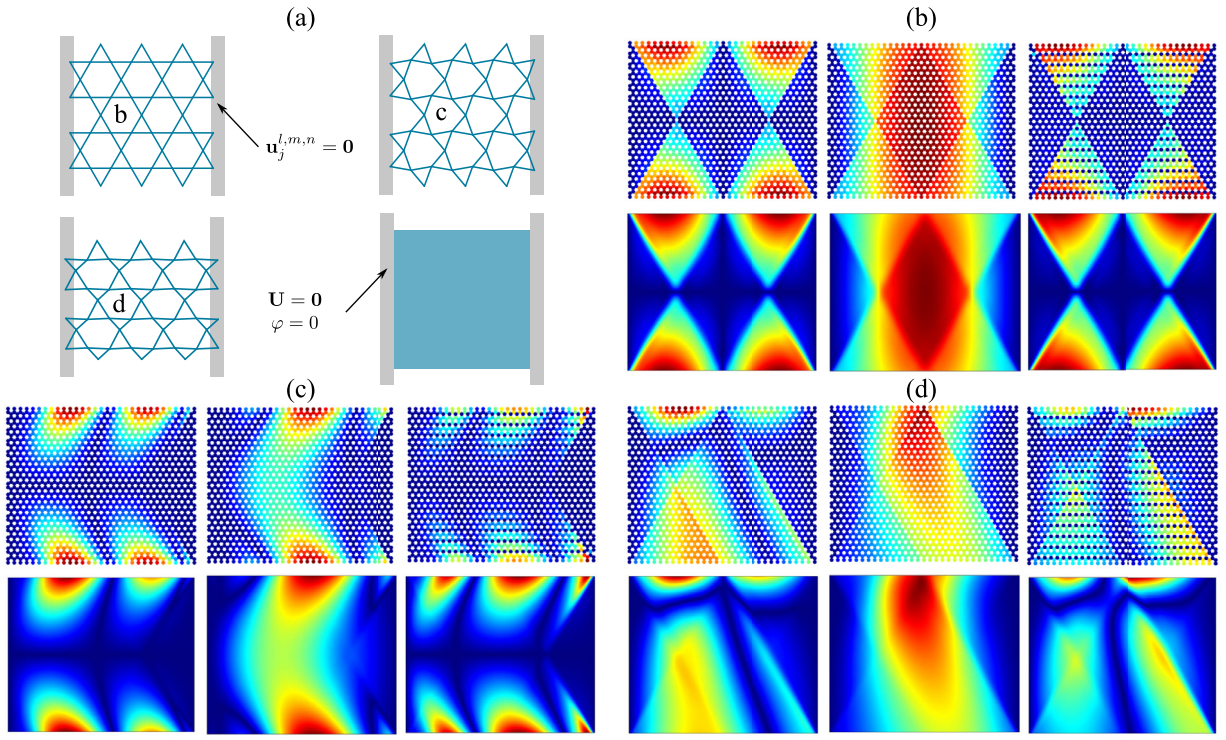

Fig. 6. Comparison of fundamental near-zero mode prediction from lattice model and microtwist model for three different lattices: (a) lattice geometry and imposed boundary conditions; (b-d) mode shape for the discrete (top) and the continuum (bottom) models resolved into the three components U_x (left), U_y (middle) and φ (right). The distortion parameters are: (b) $w_j = 0$; (c) $w_j/a_j = -4\%$; (d) $w_1/a_1 \approx 1.7\%$, $w_2/a_2 \approx -0.87\%$ and $w_3/a_3 \approx 4.36\%$.

Equivalently, zero modes produce zero strain energy: $\epsilon = 0$. Thus, in light of expression (56), zero modes only exist in the absence of elasticity in the hinges (i.e., $\kappa = 0$) and, in that case, are solutions to

$$a_j \mathbf{e}_{jj} : \boldsymbol{\nabla}^s \mathbf{U} + \frac{ah}{3} \mathbf{e}_j \cdot \boldsymbol{\nabla} \varphi + \gamma w_j \varphi = 0, \quad j = 1, 2, 3. \tag{73}$$

The above system of linear partial differential equations provides a continuum characterization of the zero modes of regular and weakly-distorted Kagome lattices. As a sanity check, note that this characterization is independent of the elastic moduli k_j, zero modes being representative of configurations that do not stretch any bonds.

It is possible to numerically solve the above system under appropriate boundary conditions. Alternatively, it is more convenient to obtain *approximate* zero modes by minimizing strain energy in the presence of a small residual elastic energy stored in the hinges (i.e., for $0 < \kappa \sim 0$). Thus, we consider a rectangular sample freely vibrating under Dirichlet left and right boundary conditions and free top and bottom boundaries as shown on Fig. 6a. We then calculate the eigenmode of lowest energy for both the discrete and continuum models. This fundamental eigenmode becomes a zero mode in the limit $\kappa \to 0$. Three components corresponding to U_x, U_y and φ are extracted from the eigenmode's shape and are plotted as normalized color maps on Fig. 6b-d for three different lattices. In all of these cases, the microtwist continuum predicts well the mode shape of the approximate zero mode.

It is of interest here to highlight how the distortion parameters w_j influence the space distribution of zero modes. On plot (b), the w_j are all null, and the zero mode reaches deep into the bulk of the sample. This is consistent with the fact that regular lattices admit bulk Floquet-Bloch zero modes. On plot (c), the w_j are all of the same sign, namely positive; the zero mode is localized near edges and decays exponentially towards the bulk. Again, this is consistent with the fact that geometric distortions gap Floquet-Bloch zero modes at non-zero wavenumbers. Last, on plot (d), where $w_j \neq 0$ but not all of the same sign, namely w_1, $w_3 > 0$ and $w_2 < 0$, the zero mode localizes again near edges but does so in an asymmetric fashion: the zero mode appears to favor the top edge over the bottom one. This phenomenon of polarization is a symptom of the loss of P-symmetry; it is ubiquitous in distorted Kagome lattices but is most pronounced in those lattices qualified as "topological" by Kane and Lubensky (2014). Hereafter, we analyze in more detail the polarized distribution of zero modes in distorted Kagome lattices as well as the notions of "topology" and "topological polarization".

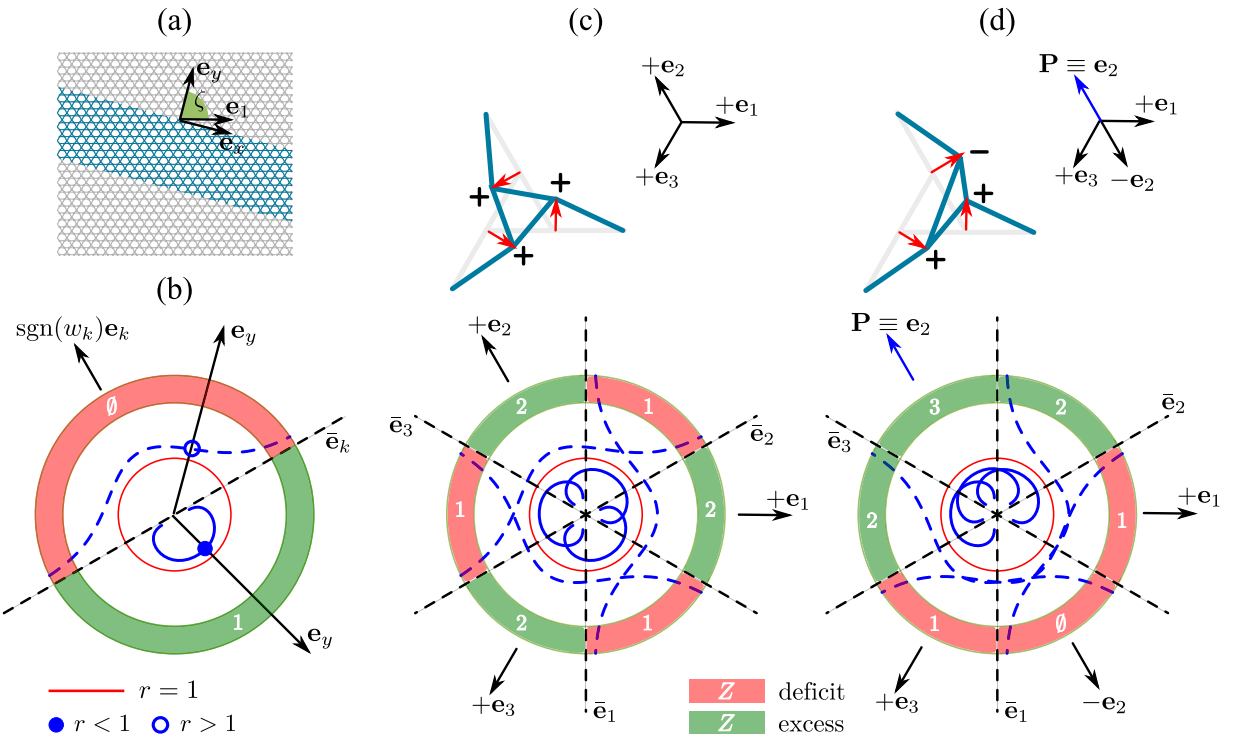

Fig. 7. Polar plots of the decay factor $r = r(\mathbf{e}_y)$: (a) Geometry of a finite slice of an infinite lattice; (b) Generic plot of r for branch k of Eq. (80); dashed (resp. solid) lines correspond to $r > 1$ (resp. $r < 1$); two antipodal points correspond to two opposite surfaces; sectors are color-coded to indicate when a surface exhibits an excess or a deficit of zero modes compared to the opposite surface. (c, d) Generic plots of r for when all branches are superposed; the top shows example unit cells with exaggerated distortions and relative orientation of vectors $\mathbf{e}_j$ and $\mathrm{sgn}(w_j)\mathbf{e}_j = \pm\mathbf{e}_j$; the signs correspond to the signs of the w_j. The bottom shows the polar plots. In the trivial configuration (c), sectors with an excess of zero modes are disconnected; that is, $\mathbf{P} = \mathbf{0}$. In the topological configuration (d), these sectors are adjacent with all corresponding $\mathbf{e}_y$ making acute angles with $\mathbf{P} = \mathbf{e}_2$.

5.3. Polarization effects in the distribution of zero modes

Consider a distorted lattice such that all w_j are non-zero. Therein, zero modes of a non-zero wavenumber $\mathbf{q}$ are necessarily localized. Suppose then that in the (x, y)-plane of basis $(\mathbf{e}_x, \mathbf{e}_y)$, the lattice occupies a band $-Y < y < 0$ of a finite width Y and of infinite length in the x-direction with $\mathbf{e}_y$ inclined with respect to $\mathbf{e}_1$ by some angle ζ (Fig. 7a). A zero mode localized near the top boundary $y = 0$ exhibits a wavenumber $\mathbf{q} = q_x\mathbf{e}_x + q_y\mathbf{e}_y$ where q_x is real and non-zero and $q_y = q_R + iq_I$ is complex with real part q_R and a negative non-zero imaginary part q_I. Hence, the zero mode maintains a constant amplitude in the x-direction but decays exponentially in the y-direction. Conversely, a mode localized near the bottom boundary $y = -Y$ has $q_I > 0$.

Given q_x, component q_y can be determined by solving a complex dispersion relation. To find it, specify the field Eqs. (73) to a plane wave of amplitude $(\mathbf{U}_o, \varphi_o)$. Eqs. (73) then yield

$$ia_j\langle\mathbf{e}_j, \mathbf{q}\rangle\langle\mathbf{e}_j, \mathbf{U}_o\rangle + \left(i\frac{ah}{3}\langle\mathbf{e}_j, \mathbf{q}\rangle + \gamma w_j\right)\varphi_o = 0, \quad j = 1, 2, 3. \tag{74}$$

Non-trivial solutions exist when the zero-determinant condition

$$\det\begin{bmatrix} ia_1\langle\mathbf{e}_1, \mathbf{q}\rangle\mathbf{e}_1' & i\frac{ah}{3}\langle\mathbf{e}_1, \mathbf{q}\rangle + \gamma w_1 \\ ia_2\langle\mathbf{e}_2, \mathbf{q}\rangle\mathbf{e}_2' & i\frac{ah}{3}\langle\mathbf{e}_2, \mathbf{q}\rangle + \gamma w_2 \\ ia_3\langle\mathbf{e}_3, \mathbf{q}\rangle\mathbf{e}_3' & i\frac{ah}{3}\langle\mathbf{e}_3, \mathbf{q}\rangle + \gamma w_3 \end{bmatrix} = 0 \tag{75}$$

is met. Equivalently, q_y is solution to the complex dispersion relation

$$ah\prod_j\langle\mathbf{e}_j, \mathbf{q}\rangle - i\gamma\sum_j w_j\prod_{k\neq j}\langle\mathbf{e}_k, \mathbf{q}\rangle = 0. \tag{76}$$

Generally speaking, the above equation is polynomial of degree 3 and therefore admits three complex solutions. A key observation here is that an odd number of zero modes, namely 3, cannot be evenly split between the top and bottom boundaries. Thus, the top or the bottom must exhibit a relative excess or deficit in the number of zero modes they host.

In other words, if the top boundary hosts Z zero modes out of the available three, then the bottom boundary hosts the remaining $3-Z$, and Z cannot equal $3-Z$. This is, at its simplest, where polarization effects come from.

5.4. Trivial and topological polarization

From now on, we will refer to the boundary $y=0$ as the surface of normal $\mathbf{e}_y$. We equally refer to the opposite surface $y=-Y$ by its outward normal $-\mathbf{e}_y$. It is of interest to determine for which normal vectors $\mathbf{e}_y$, will the surface host a relative excess or deficit in zero modes compared to the opposite surface. To do so, we look for particularly simple solutions to (76) such that $\mathbf{q}$ is dominantly imaginary, i.e., highly localized in the y-direction in comparison to its oscillatory components in the x- and y-directions (i.e., $q_I \gg q_R, q_x$). In that case, to leading order, $\mathbf{q} \sim iq_I\mathbf{e}_y$ implies

$$-iahq_I^3 \prod_j \langle \mathbf{e}_j, \mathbf{e}_y \rangle + iq_I^2\gamma \sum_j w_j \prod_{k\neq j} \langle \mathbf{e}_k, \mathbf{e}_y \rangle = 0, \tag{77}$$

and

$$q_I = \frac{\gamma}{ah} \sum_j \frac{w_j}{\langle \mathbf{e}_j, \mathbf{e}_y \rangle}. \tag{78}$$

The above solution is only accurate if consistent with the premise of high localization, i.e., only in the vicinity of normal directions such that

$$\langle \mathbf{e}_j, \mathbf{e}_y \rangle = 0 \tag{79}$$

for some $j=k$. Accordingly, the particular solution further simplifies into

$$q_I = \frac{\gamma}{ah} \frac{w_k}{\langle \mathbf{e}_k, \mathbf{e}_y \rangle}. \tag{80}$$

It is insightful to vary $\mathbf{e}_y$ around the unit circle and draw a generic polar plot $r = r(\mathbf{e}_y)$ of the decay factor $r = \exp(q_I/q_x)$, where q_x, taken positive, is used as a normalization factor; see Fig. 7b. Factor r quantifies for each surface of normal $\mathbf{e}_y$, how fast the zero mode's amplitude decays in the y-direction taking the wavelength in the x-direction as a reference. Thanks to the derived particular solutions, we know that r approaches 0 in directions $\mathbf{e}_y$ that are close to $\pm\bar{\mathbf{e}}_k$ but make an *obtuse* angle with $\mathrm{sgn}(w_k)\mathbf{e}_k$. By contrast, r approaches $+\infty$ in directions $\mathbf{e}_y$ that are close to $\pm\bar{\mathbf{e}}_k$ but make an *acute* angle with $\mathrm{sgn}(w_k)\mathbf{e}_k$. Between these extremes, r has a continuous profile that never reaches 1. Indeed, $r=1$ corresponds to a zero mode with $\mathbf{q}$ real and non-zero that do not exist when all distortion parameters w_j are non-zero.

There exists of course one such branch for each k exemplified on Fig. 7b. Combining the various branches for $k=1,2,3$, it is possible to count the number of zero modes Z hosted by a surface of normal $\mathbf{e}_y$: it is equal to the number of branches such that $r<1$ in direction $\mathbf{e}_y$. When $Z \geq 2$, the surface exhibits an excess of zero modes compared to the opposite surface; when $Z \leq 1$, the surface exhibits a deficit of zero modes compared to the opposite surface. Then, two qualitatively different configurations arise and are depicted on Fig. 7c and d. In both configurations, the normal vectors $\mathbf{e}_y$ to surfaces in possession of an excess of zero modes span three angular sectors with a total angle equal to π. In the first configuration (plot c) these sectors are disconnected; this occurs when the w_j are all of the same sign. We refer to such lattices as *trivially polarized*. In the second configuration (plot d), said sectors are adjacent; this occurs when the w_j are not all of the same sign. We refer to these lattices as *topologically polarized*.

While either way the lattice is polarized, topologically polarized lattices are expected to exhibit stronger polarization effects. Indeed, in such lattices, it is possible to find a unitary polarization vector $\mathbf{P}$ such that $\langle \mathbf{e}_y, \mathbf{P} \rangle > 0$ if and only if the surface of normal $\mathbf{e}_y$ exhibits an excess of zero modes relative to the opposite surface of normal $-\mathbf{e}_y$. In other words, in topologically polarized lattices, there exists a vector $\mathbf{P}$ which systematically points[6] towards the side of a lattice with the most zero modes localized near it; this vector is readily visible on Fig. 7d. In trivially polarized lattices, such a vector $\mathbf{P}$ cannot be defined; in that case $\mathbf{P}$ is by default set to $\mathbf{0}$.

Polarization $\mathbf{P}$, be it zero or not, is an example of a "topological invariant", i.e., a quantity that is robust against small and continuous perturbations. For instance, $\mathbf{P}$ is independent of the real component q_x. It is also independent of the particular geometric and constitutive parameters of the underlying lattice. Moreover, it only depends on the distortions w_j through their signs. As a matter of fact, should w_k have an opposite sign to the other two w_j, then $\mathbf{P} = -\mathrm{sgn}(w_k)\mathbf{e}_k$. Hence, for $\mathbf{P}$ to change values, some w_j has to change signs. However, given that the w_j are initially non-zero, small-enough perturbations cannot change their signs.

The above discussion justifies why lattices with $\mathbf{P} \neq \mathbf{0}$ have been qualified as "topologically polarized". On the other hand, lattices with $\mathbf{P} = \mathbf{0}$ are "topologically non-polarized"; yet, they are polarized in the sense that they are P-asymmetric. Hence, we preferred to refer to them as "trivially polarized". Last, the excluded lattices with some $w_j = 0$ are in a critical state such that any perturbation, however small, can lead to a trivially or a topologically polarized state depending on the sign of w_j post-perturbation. Thus, polarization effects in such lattices are very sensitive to perturbations; they do not feature any topological qualities.

[6] In the sense that it makes an acute angle with the outward normal.

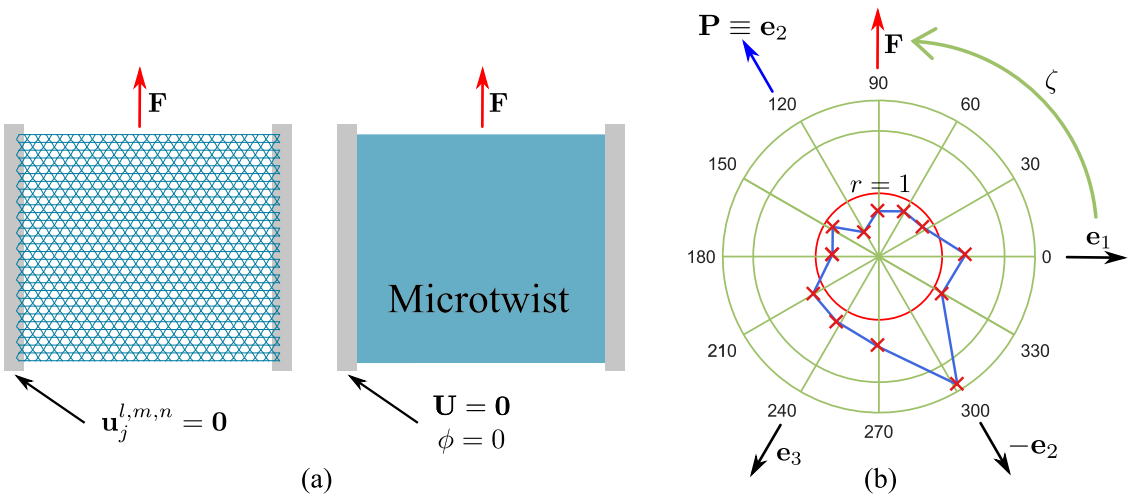

Fig. 8. Indentation tests simulated for free surfaces of different inclinations ζ: (a) boundary conditions; (b) polar plot of the relative surface stiffness; the crosses (resp. solid line) correspond to the continuum (resp. discrete) model. Configuration (a) corresponds to $\zeta = \pi/2$. Distortion parameters are $w_1/a_1 \approx 1.7\%$, $w_2/a_2 \approx -0.87\%$ and $w_3/a_3 \approx 4.36\%$.

Note that this macroscopic notion of topological polarization is only valid in the limit of small distortions w_j. For large enough w_j, zero modes localize over thin boundary layers and can no longer be captured using the present continuum theory, not in its current form at least. Based on a study of the discrete lattice, Kane and Lubensky (2014) introduced and interpreted a topological polarization vector $\mathbf{P}^{KL}$ which similarly serves to pinpoint free surfaces with an excess of zero modes. Their analysis led to the elegant formula

$$\mathbf{P}^{KL} = -\frac{1}{2}\sum_k \operatorname{sgn}(w_k)\mathbf{r}_k. \tag{81}$$

Retrieving $\mathbf{P}^{KL}$ on a macroscopic level was a principal motivation behind the present work. Indeed, it is straightforward to check that $\mathbf{P}^{KL}$ and $\mathbf{P}$ are colinear. That being said, it is important to stress that $\mathbf{P}^{KL}$ and $\mathbf{P}$ do not count the same zero modes. Specifically, the construction of $\mathbf{P}$ is based on counting macroscopic zero modes, i.e., those zero modes which decay or grow slow enough across many unit cells so as to survive a micro-to-macro scale transition. Vector $\mathbf{P}^{KL}$ on the other hand takes into account all zero modes however localized.

5.5. Indentation tests

Asymmetric distributions of zero modes cause a polarized elastic response. Here, we investigate the polarized elastic response of a topologically polarized lattice and assess whether the microtwist theory is capable of accurately reproducing that response on a macroscopic level.

Consider a rectangular sample of a topologically polarized lattice where the top and bottom edges are free and the left and right edges are constrained. Like before, we let $\mathbf{e}_y$ be the outward unit normal along the top edge and call ζ the angle it makes with $\mathbf{e}_1$; vector $\mathbf{e}_x$ is aligned with the free edge. For angles ζ sweeping the range $[0, 2\pi)$, we apply an outward force $\mathbf{F}$ at the midpoint of the top edge and calculate, using FEA, the displacement at the same point where the force is applied (Fig. 8a). The ratio of the force to the y-displacement defines a surface stiffness $S(\zeta)$; the polar plot $r(\zeta) = S(\zeta)/S(\zeta + \pi)$ compares the stiffnesses of the top and bottom edges and allows to gauge how polarized the elastic response is: for a given inclination ζ, a relative stiffness $r > 1$ means that the top surface is stiffer than the bottom surface. A similar plot is made using the microtwist continuum. The two plots match satisfyingly (Fig. 8b).

For this particular example, $\mathbf{P} = \mathbf{e}_2$ since w_2 is negative whereas w_1 and w_3 are positive. Thus, zero modes overpopulate edges where the outward unit normal forms an acute angle with $\mathbf{P}$. These correspond to angles ζ between 30° and 210°, approximately. For all of these angles, the relative surface stiffness is lower than 1 signaling a relative softening of these edges. Maximum softening is reached in the direction of $\mathbf{P}$, approximately. It is worth noting here, that in order to guarantee the well-posedness of the indentation problem, simulations are performed in the presence of a small residual elasticity in the hinges $0 < \kappa \sim 0$.

6. Conclusion

In this paper, we developed a theory of elasticity, called microtwist elasticity, that can capture the zero modes and topological polarization of Kagome lattices on a macroscopic scale. Performance of the proposed theory is validated against

the discrete model in a number of problems including determining the P-asymmetric distribution of zero modes, calculating the dispersion relations and quantitatively predicting the polarized indentation response of finite samples. The theory also permits to establish a classification of isostatic Kagome lattices function of their distortion and polarization.

The theory extends easily to nearly-isostatic Kagome lattices, i.e., with next-nearest-neighbor interactions or elasticity in the hinges, as long as the elastic constants of the bonds breaking isostaticity are kept small. It also extends to other isostatic lattices that are on the brink of a regular-distorted, or polarized-unpolarized, phase transition.

It is of interest to see if and how the theory could be applied to strongly distorted lattices in connection to the work of Sun and Mao (2019), of Saremi and Rocklin (2020) and of Marigo and Maurel (2016, 2017). It is equally interesting to explore how polarization influences the dynamic behavior and to investigate the role of the coupling measure of microinertia $\rho\bar{\mathbf{d}}$. On a more fundamental level, potential corrections brought by microtwist elasticity to the models of strength of materials (e.g., bending and torsion of beams) widely used by engineers are worthy of investigation in cases where the constitutive materials are lattice-like. Finally, experimental efforts characterizing the polarized behavior of such lattice materials are much needed.

Declaration of Competing Interest

The authors declare no conflict of interest.

CRediT authorship contribution statement

Hussein Nassar: Conceptualization, Formal analysis, Methodology, Funding acquisition, Writing - review & editing. **Hui Chen:** Conceptualization, Formal analysis, Methodology, Writing - review & editing. **Guoliang Huang:** Conceptualization, Validation, Supervision, Funding acquisition, Writing - review & editing.

Acknowledgments

This work is supported by the NSF CMMI under Award No. 1930873 with Program Manager Dr. Nakhiah Goulbourne, the Air Force Office of Scientific Research under Grant No. AF 9550-18-1-0342 with Program Manager Dr. Byung-Lip (Les) Lee and the Army Research Office under Grant No. W911NF-18-1-0031 with Program Manager Dr. Daniel P. Cole. The authors would like to thank the anonymous reviewers for useful suggestions and Samuel Forest (CNRS, Mines-ParisTech) for helpful discussion.

Appendix A. The rank of the compatibility matrix

We have seen that, for periodic configurations in a general Kagome lattice, the compatibility matrix reads

$$C_0 = \begin{bmatrix} \mathbf{0} & -\mathbf{m}_1' & \mathbf{m}_1' \\ \mathbf{m}_2' & \mathbf{0} & -\mathbf{m}_2' \\ -\mathbf{m}_3' & \mathbf{m}_3' & \mathbf{0} \\ \mathbf{0} & -\mathbf{n}_1' & \mathbf{n}_1' \\ \mathbf{n}_2' & \mathbf{0} & -\mathbf{n}_2' \\ -\mathbf{n}_3' & \mathbf{n}_3' & \mathbf{0} \end{bmatrix}. \tag{82}$$

By the rank-nullity theorem, the number of zero modes is equal to $Z = 6 - \text{rank}C_0$ where 6 is the dimension of C_0 and $\text{rank}C_0$ its rank. On one hand, translations systematically provide two linearly independent periodic zero modes so that $Z \geq 2$. On the other hand, the first three lines of matrix C are necessarily linearly independent because, for instance, $\mathbf{m}_2$ and $\mathbf{m}_3$ can never be parallel. Thus, $\text{rank}C \geq 3$ leaving us with two possibilities: $(Z, \text{rank}C_0) = (2, 4)$ or (3,3).

If there exists a j such that $\mathbf{m}_j$ and $\mathbf{n}_j$ are misaligned, then $Z = 2$. Indeed, say, for the sake of argument, that $j = 1$. Then, the extracted 4×4 matrix

$$\begin{bmatrix} -\mathbf{m}_1' & \mathbf{m}_1' \\ \mathbf{0} & -\mathbf{m}_2' \\ \mathbf{m}_3' & \mathbf{0} \\ -\mathbf{n}_1' & \mathbf{n}_1' \end{bmatrix} \tag{83}$$

has a non-zero determinant since otherwise $\mathbf{m}_2$ and $\mathbf{m}_3$ would be aligned. Therefore, C_0 is of rank 4 and $Z = 2$. In contrast, if for all j, $\mathbf{m}_j$ and $\mathbf{n}_j$ are parallel, then $Z = 3$. As a matter of fact, $\mathbf{m}_j$ and $\mathbf{n}_j$ being aligned and unitary means they are equal and opposite. In that case, the last three lines of C_0 are exactly the opposites of the first three ones and the rank of C_0 cannot exceed its lower bound of 3 nor can Z decrease below its upper bound of 3.

Appendix B. Existence of Floquet-Bloch zero modes

In the main text, it was proven that a Floquet-Bloch zero mode of wavenumber $\mathbf{q}$ such that $Q_j = 1$ exists if and only if $\mathbf{m}_j = -\mathbf{n}_j$. But then it is unclear whether other solutions exist where $Q_j \neq 1$ for all j. Here, we provide a sufficient condition under which there exist no solutions to (23) outside of the lines $Q_j = 1$.

Thus, let $\mathbf{q}$ be a real wavenumber such that $Q_j \neq 1$ for all j. Divide (23) by $\prod_j (1 - Q_j)$ yielding

$$\sum_j \left\langle b_j \mathbf{n}_j, \tilde{\mathbf{x}}_{j+1} \right\rangle + \sum_j \frac{\left\langle b_j \mathbf{n}_j, a_j \bar{\mathbf{m}}_j \right\rangle}{1 - Q_j} = 0. \tag{84}$$

Upon extracting the real part of this complex equation, it comes that

$$\sum_j \left\langle b_j \mathbf{n}_j, \tilde{\mathbf{x}}_{j+1} \right\rangle + \sum_j \frac{\left\langle b_j \mathbf{n}_j, a_j \bar{\mathbf{m}}_j \right\rangle}{2} = 0. \tag{85}$$

Now let A_m, A_n and A_r be the areas of the triangles $(a_1\mathbf{m}_1, a_2\mathbf{m}_2, a_3\mathbf{m}_3)$, $(b_1\mathbf{n}_1, b_2\mathbf{n}_2, b_3\mathbf{n}_3)$ and $(\mathbf{r}_1, \mathbf{r}_2, \mathbf{r}_3)$; in particular $A_r = A/2$ is half of the area of a unit cell. Following some elementary algebraic manipulations, the above equation remarkably turns out to be equivalent to

$$A_m + A_n = A_r. \tag{86}$$

In conclusion, in any Kagome lattice where $A_m + A_n \neq A_r$, there exist no Floquet-Bloch zero modes with $\mathbf{q}$ outside of the lines $Q_j = 1$. This holds in particular for lattices that are not "too distorted" where $A_m + A_n < A_r$. In particular, weakly-distorted lattices such that all w_j are non-zero are gapped at zero frequency except at the origin $\mathbf{q} = \mathbf{0}$.

Appendix C. Influence of elasticity in the hinges

Adding rotational springs so as to account for elasticity in the hinges is arguably equivalent to adding next-nearest-neighbor interactions between nodes. Both have a stabilizing effect on the lattice and will block twisting motions leaving translations as the only periodic zero modes. When the rotational spring constants are comparable to or higher than the effective spring constants k_j, the Kagome lattice will be far from the regular-distorted phase transition regime of interest. Its study, from a homogenization point of view, can thus be done using standard tools as described by Hutchinson and Fleck (2006) or by Lubensky et al. (2015) for instance and will not be pursued here. Instead, focus will be on lattices where the rotational spring constants are much smaller than k_j, specifically, where they are of second order compared to k_j since such lattices will be on the brink of a regular-distorted phase transition.

Formally, the expansion of the motion Eq. (44) will change so as to include an additional second-order term $C_H'\delta^2 K_H C_H \Phi_0$ due to the presence of elasticity in the hinges. Therein, C_H is the periodic compatibility matrix corresponding to the rotational springs or equivalently to the next-nearest-neighbor bonds whereas $\delta^2 K_H$ is the corresponding matrix of elastic constants. This term is only relevant in the last step of the homogenization theory where the corrections $D'C_H'\delta^2 K_H C_H \Phi_0$ and $T'C_H'\delta^2 K_H C_H \Phi_0$ need to be added to the macroscopic motion equations. However, the former of these two corrections is zero whereas the latter is proportional to φ. This is because translations remain periodic zero modes: $C_H D = 0$. Accordingly, the effective constitutive law remains the same as without elasticity in the hinges up to changing the effective parameter L into

$$L = \kappa + \frac{\gamma^2}{ah} \sum_j w_j^2 k_j \tag{87}$$

with $\kappa = T'C_H'\delta^2 K_H C_H T/A$ and A being the unit cell area.

References

Allaire, G., Palombaro, M., Rauch, J., 2011. Diffractive geometric optics for Bloch wave packets. Arch. Ration. Mech. Anal. 202, 373–426.
Auffray, N., Bouchet, R., Bréchet, Y., 2010. Strain gradient elastic homogenization of bidimensional cellular media. Int. J. Solids Struct. 47, 1698–1710.
Bacigalupo, A., Gambarotta, L., 2014. Homogenization of periodic hexa- and tetrachiral cellular solids. Compos. Struct. 116, 461–476.
Bensoussan, A., Lions, J.L., Papanicolaou, G., 1978. Asymptotic Analysis for Periodic Structures. North-Holland Publishing Company.
Bilal, O.R., Süsstrunk, R., Daraio, C., Huber, S.D., 2017. Intrinsically polar elastic metamaterials. Adv. Mater. 29, 1700540.
Birkhoff, G., MacLane, S., 1998. A survey of Modern Algebra. Taylor and Francis.
Chen, Y., Liu, X.N., Hu, G.K., 2014. Micropolar modeling of planar orthotropic rectangular chiral lattices. Comptes Rendus Mec. 342, 273–283.
Craster, R.V., Kaplunov, J., Pichugin, A.V., 2010. High-frequency homogenization for periodic media. Proc. R. Soc. A 466, 2341–2362.
Dresselhaus, M.S., Dresselhaus, G., Jório, A., 2008. Group Theory: Application to the Physics of Condensed Matter. Springer-Verlag Berlin Heidelberg.
Eringen, A.C., 1999. Microcontinuum Field Theories I: Foundations and Solids. Springer, New York.
Forest, S., Sievert, R., 2006. Nonlinear microstrain theories. Int. J. Solids Struct. 43, 7224–7245.
Frenzel, T., Kadic, M., Wegener, M., 2017. Three-dimensional mechanical metamaterials with a twist. Science 358, 1072–1074.
Harutyunyan, D., Milton, G.W., Craster, R.V., 2016. High-frequency homogenization for travelling waves in periodic media. Proc. R. Soc. A 472, 20160066.
Hutchinson, R.G., Fleck, N.A., 2006. The structural performance of the periodic truss. J. Mech. Phys. Solids 54, 756–782.
Kane, C.L., Lubensky, T.C., 2014. Topological boundary modes in isostatic lattices. Nat. Phys. 10, 39–45.
Lakes, R.S., 1987. Foam structures with a negative Poisson's ratio. Science 235, 1038–1040.
Lakes, R.S., 2001. Elastic and viscoelastic behavior of chiral materials. Int. J. Mech. Sci. 43, 1579–1589.

Lakes, R.S., Benedict, R.L., 1982. Noncentrosymmetry in micropolar elasticity. Int. J. Eng. Sci. 20, 1161–1167.
Liu, X.N., Huang, G.L., Hu, G.K., 2012. Chiral effect in plane isotropic micropolar elasticity and its application to chiral lattices. J. Mech. Phys. Solids 60, 1907–1921.
Lubensky, T.C., Kane, C.L., Mao, X.M., Souslov, A., Sun, K., 2015. Phonons and elasticity in critically coordinated lattices. Reports Prog. Phys. 78, 073901.
Makwana, M., Antonakakis, T., Maling, B., Guenneau, S., Craster, R.V., 2016. Wave mechanics in media pinned at Bravais lattice points. SIAM J. Appl. Math. 76, 1–26.
Mao, X.M., Lubensky, T.C., 2018. Maxwell lattices and topological mechanics. Annu. Rev. Condens. Matter Phys. 9, 413–433.
Marigo, J.J., Maurel, A., 2016. Homogenization models for thin rigid structured surfaces and films. J. Acoust. Soc. Am. 140, 260–273.
Marigo, J.J., Maurel, A., 2017. Second order homogenization of subwavelength stratified media including finite size effect. SIAM J. Appl. Math. 77, 721–743.
Milton, G.W., 2013. Adaptable nonlinear bimode metamaterials using rigid bars, pivots, and actuators. J. Mech. Phys. Solids 61, 1561–1568.
Milton, G.W., 2013. Complete characterization of the macroscopic deformations of periodic unimode metamaterials of rigid bars and pivots. J. Mech. Phys. Solids 61, 1543–1560.
Milton, G.W., Cherkaev, A.V., 1995. Which elasticity tensors are realizable? J. Eng. Mater. Technol. 117, 483.
Mindlin, R.D., 1964. Micro-structure in linear elasticity. Arch. Ration. Mech. Anal. 16, 51–78.
Nassar, H., Chen, Y.Y., Huang, G.L., 2018. A degenerate polar lattice for cloaking in full two-dimensional elastodynamics and statics. Proc. R. Soc. A 474, 20180523.
Nassar, H., Chen, Y.Y., Huang, G.L., 2019. Isotropic polar solids for conformal transformation elasticity and cloaking. J. Mech. Phys. Solids 129, 229–243.
Nassar, H., Chen, Y.Y., Huang, G.L., 2020. Polar metamaterials: a new outlook on resonance for cloaking applications. Phys. Rev. Lett. 124, 84301.
Nassar, H., Lebée, A., Monasse, L., 2017. Curvature, metric and parametrization of origami tessellations: theory and application to the eggbox pattern. Proc. R. Soc. A 473, 20160705.
Nassar, H., Lebée, A., Monasse, L., 2018. Fitting surfaces with the Miura tessellation. In: Lang, R.J., Bolitho, M., You, Z. (Eds.), Origami 7. Oxford, pp. 811–826.
Norris, A.N., 2008. Acoustic cloaking theory. Proc. R. Soc. A 464, 2411–2434.
Peraza-Hernandez, E.A., Hartl, D.J., Malak Jr, R.J., Lagoudas, D.C., 2014. Origami-inspired active structures: a synthesis and review. Smart Mater. Struct. 23, 094001.
Rocklin, D.Z., 2017. Directional mechanical response in the bulk of topological metamaterials. New J. Phys. 19, 065004.
Rocklin, D.Z., Zhou, S.N., Sun, K., Mao, X.M., 2017. Transformable topological mechanical metamaterials. Nat. Commun. 8, 14201.
Rosi, G., Auffray, N., 2016. Anisotropic and dispersive wave propagation within strain-gradient framework. Wave Motion 63, 120–134.
Rus, D., Tolley, M.T., 2018. Design, fabrication and control of origami robots. Nat. Rev. Mater. 3, 101–112.
Saremi, A., Rocklin, D.Z., 2020. Topological elasticity of flexible structures. Phys. Rev. X 10, 011052.
Spadoni, A., Ruzzene, M., 2012. Elasto-static micropolar behavior of a chiral auxetic lattice. J. Mech. Phys. Solids 60, 156–171.
Sun, K., Mao, X.M., 2019. Continuum theory for topological edge soft modes. Phys. Rev. Lett. 124, 207601.
Sun, K., Souslov, A., Mao, X.M., Lubensky, T.C., 2012. Surface phonons, elastic response, and conformal invariance in twisted kagome lattices. Proc. Natl. Acad. Sci. U. S. A. 109, 12369–12374.
Xu, X.C., Wang, C., Shou, W., Du, Z.L., Chen, Y.Y., Li, B., Matusik, W., Nassar, H., Huang, G.L., 2020. Physical realization of elastic cloaking with a polar material. Phys. Rev. Lett. 124, 114301.